© 2016. Published by The Company of Biologists Ltd | Development (2016) 143, 4236-4248 doi:10.1242/dev.139642

RESEARCH ARTICLE

Constitutive expression of microRNA-150 in mammary epithelium suppresses secretory activation and impairs *de novo* lipogenesis

Richard E. Heinz[1], Michael C. Rudolph[2], Palani Ramanathan[3], Nicole S. Spoelstra[4], Kiel T. Butterfield[4], Patricia G. Webb[5], Beatrice L. Babbs[4], Hongwei Gao[6], Shang Chen[6], Michael A. Gordon[4], Steve M. Anderson[4], Margaret C. Neville[5,7], Haihua Gu[6,4,*] and Jennifer K. Richer[4,*]

ABSTRACT

Profiling of RNA from mouse mammary epithelial cells (MECs) isolated on pregnancy day (P)14 and lactation day (L)2 revealed that the majority of differentially expressed microRNA declined precipitously between late pregnancy and lactation. The decline in miR-150, which exhibited the greatest fold-decrease, was verified quantitatively and qualitatively. To test the hypothesis that the decline in miR-150 is crucial for lactation, MEC-specific constitutive miR-150 was achieved by crossing *ROSA26-lox-STOP-lox-miR-150* mice with WAP-driven Cre recombinase mice. Both biological and foster pups nursed by bitransgenic dams exhibited a dramatic decrease in survival compared with offspring nursed by littermate control dams. Protein products of predicted miR-150 targets *Fasn*, *Olah*, *Acaca*, and *Stat5B* were significantly suppressed in MECs of bitransgenic mice with constitutive miR-150 expression as compared with control mice at L2. Lipid profiling revealed a significant reduction in fatty acids synthesized by the *de novo* pathway in L2 MECs of bitransgenic versus control mice. Collectively, these data support the hypothesis that a synchronized decrease in miRNAs, such as miR-150, at late pregnancy serves to allow translation of targets crucial for lactation.

KEY WORDS: MicroRNA-150, Lactation, Mammary gland, Fatty acid synthesis

INTRODUCTION

During post-pubertal mammary gland (MG) development, coordinated transcriptional changes directed primarily by estrogen, progesterone and prolactin and their respective receptors govern progression through pregnancy to lactation and involution (Rudolph et al., 2003). During these stages, mammary epithelial cells (MEC) undergo massive proliferatory expansion, differentiation and secretory activation, followed by apoptosis as previously reviewed (Anderson et al., 2007).

[1]Cancer Biology Graduate Program, University of Colorado Anschutz Medical Campus, Aurora, CO 80045, USA. [2]Division of Endocrinology, Metabolism and Diabetes, School of Medicine, University of Colorado Anschutz Medical Campus, Aurora, CO 80045, USA. [3]Department of Pathology, University of Texas Medical Branch, Galveston, TX 77555, USA. [4]Department of Pathology, University of Colorado Anschutz Medical Campus, Aurora, CO 80045, USA. [5]Department of Obstetrics and Gynecology, University of Colorado Anschutz Medical Campus, Aurora, CO 80045, USA. [6]Key Laboratory of Laboratory Medicine, Ministry of Education, School of Laboratory Medicine and Life Science, Wenzhou Medical University, Wenzhou 325035, China. [7]Department of Physiology and Biophysics, University of Colorado Anschutz Medical Campus, Aurora, CO 80045, USA.

*Authors for correspondence (haihua.gu@ucdenver.edu; jennifer.richer@ucdenver.edu)

R.E.H., 0000-0003-4850-2248; H.G., 0000-0003-2154-9900; J.K.R., 0000-0002-9960-0991

Received 12 May 2016; Accepted 29 September 2016

Differentiation occurs during mid to late pregnancy in the mouse, when the MECs become competent to synthesize milk, but importantly, actual secretion is held in check until parturition when secretory activation is triggered (Rudolph et al., 2003; Anderson et al., 2007). This trigger results in copious synthesis of milk comprising milk proteins, sugars and fats. Secretory activation may be regulated, in part, at the translational level by expression of microRNAs (miRNAs) that attenuate protein synthesis until biosynthetic enzymes and secretory machinery are needed. Avril-Sassen et al. (2009) performed the first global expression array of miRNAs from whole MG lysates throughout postnatal development and found that the three most populated miRNA expression patterns shared a dramatic decline at the transition between pregnancy and lactation.

Whereas the Caldas group identified distinct patterns of miRNA expression during MG development, it is possible that other cell types such as mammary adipose, lymphatic and immune cells (Rudolph et al., 2009) contributed to the patterns observed. Therefore, to identify MEC-specific miRNAs with the potential to regulate secretory activation and the biosynthetic processes of milk production, we performed simultaneous miRNA and messenger RNA (mRNA) profiling on isolated MECs from mice at pregnancy day (P)14 and lactation day (L)2. We identified a number of miRNAs that decrease in unison between P14 and L2, including miR-150-5p, which had the largest fold-decrease. The coordinated decrease in multiple miRNAs was coincident with the reciprocal upregulation of numerous metabolic pathways crucial for lactation, including lipid modification and fatty acid synthesis noted previously (Rudolph et al., 2003). To test the functional involvement of miR-150 in secretory activation, we utilized transgenic mice that constitutively express miR-150 driven by the whey acidic protein (WAP) promoter in MECs throughout mid-pregnancy and lactation. Our finding that constitutive expression of miR-150 leads to lactation deficiency and pup mortality suggests that the decline in miR-150-5p expression in MECs at late pregnancy contributes to secretory activation, induction of lipogenic mRNA and proteins, and robust activation of *de novo* lipid synthesis in lactation.

RESULTS

Decreased expression of miRNAs between late pregnancy and early lactation

To identify candidate miRNAs that regulate secretory activation specifically in MECs following functional development, simultaneous global mRNA and mature miRNA profiling was performed (analyzed data in Table S1). Thirty-two differentially expressed miRNAs displayed a ≥twofold change between P14 and L2 (Fig. 1A), and the majority (~80%) were reduced. The observed decreases include miR-150-5p, miR-17-5p and miR-425-5p, which were validated by qRT-PCR (Fig. 1B). In addition, MEC-specific decreased expression of miR-150-5p in mammary epithelium at L2

Development (2016) 143, 4236-4248 doi:10.1242/dev.139642

compared with P14 was verified by *in situ* hybridization (ISH) (Fig. 1C).

The decline of miR-150-5p at L2 coincides with increased predicted lipogenic mRNA targets

MEC-specific mRNAs were profiled by microarray and transcripts significantly different between P14 and L2 were identified using an unpaired *t*-test (analyzed data in Table S2). Ingenuity Pathway Analysis (IPA) on upregulated transcripts identified key pathways involved in secretory activation, particularly cholesterol and lipid biosynthesis (Fig. S1), were increased between pregnancy and lactation, as would be expected. Twenty-three of the 25 significantly decreased miRNAs between P14 and L2 (Fig. 1A) were predicted to target transcripts of genes involved in lipid synthesis, which increased between P14 and L2 and included key members of the *de novo* fatty acid synthesis pathways as well as several fatty acid desaturase genes (Table S3). Notably, miR-150-5p is predicted to target more lipid synthesis genes than most other miRNA (Table S3). There were 242 TargetScan-predicted miR-150-5p targets significantly upregulated by at least 1.5-fold or greater at L2 versus P14 (top three fold-changes shown in Fig. 2A). Because v-myb avian myeloblastosis viral oncogene homolog (*Myb*) is a target of miR-150-5p in B-cells (Xiao et al., 2007), MYB protein was examined by immunohistochemistry (IHC). Although the array data found *Myb* mRNA to be unaltered, MYB protein was increased in mammary epithelium at L2 compared with P14 (Fig. 2B, top), suggesting that a decrease of miR-150-5p might relieve the inhibition on *Myb* mRNA translation at lactation, allowing MYB protein to be expressed. As the fatty acid synthase gene (*Fasn*) was increased between P14 and L2 and was a predicted target, the protein level of FASN was also confirmed by IHC (Fig. 2B, bottom). IPA analysis of the 242 upregulated predicted targets of

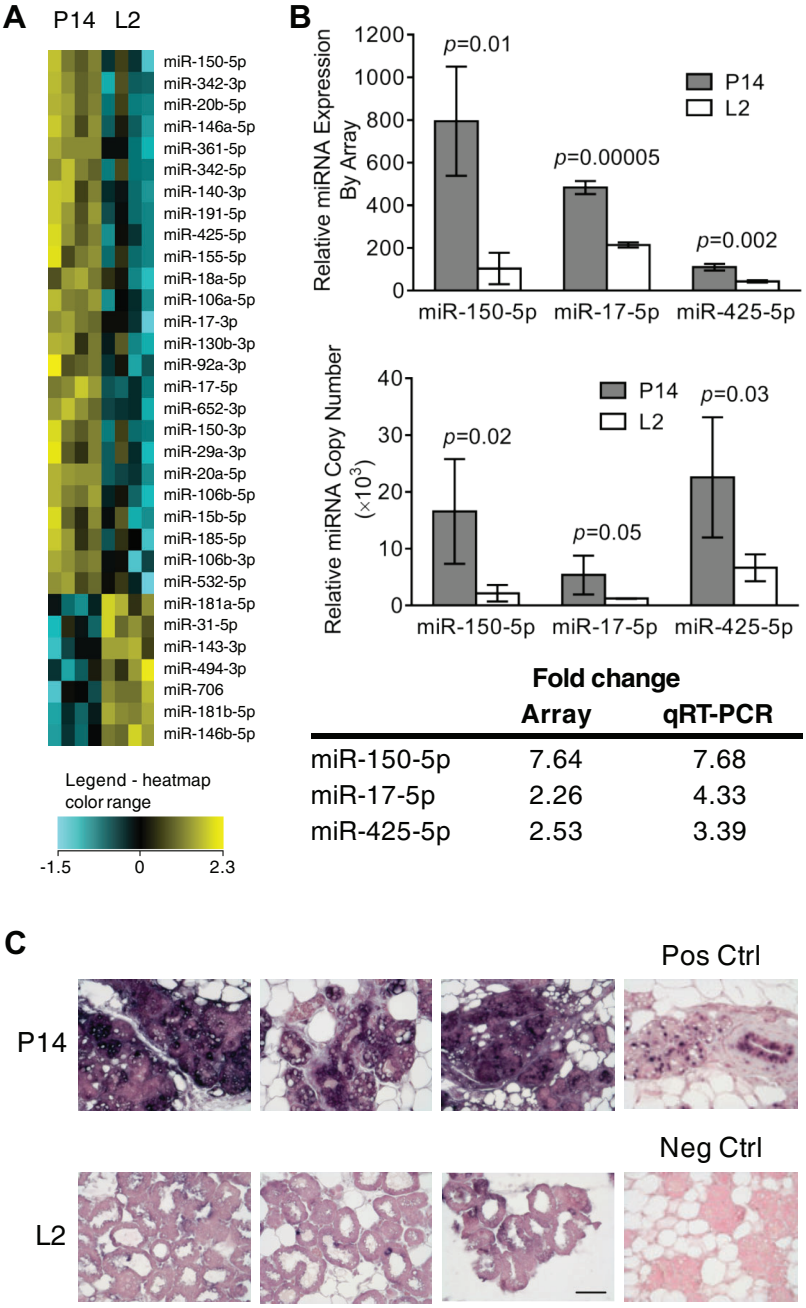

Fig. 1. Between late pregnancy and early lactation, the majority of differentially expressed miRNAs show decreased expression, with miR-150-5p demonstrating the highest fold-decrease. (A) Affymetrix GeneChip miRNA 1.0 ST array heatmap depicting normalized signal values of miRNAs with fold-change greater than two from CD1 mouse MECs at P14 and L2 (four mice per time point). Significant miRNAs sorted from most decreased in fold-change at the top to most increased at the bottom. (B) Changes in the expression of miRNAs revealed by miRNA array (top), verified by qRT-PCR (bottom). Shown are mean±s.d., n=4, unpaired t-test. Comparison of fold-change (P14/L2) between methods is shown in the table. (C) ISH analysis for mature miR-150-5p in MGs at L2 compared with P14 (three mice per time point). Positive control (RNAU6 probe) and negative control (no probe). Scale bar: 50 µm.

Development (2016) 143, 4236-4248 doi:10.1242/dev.139642

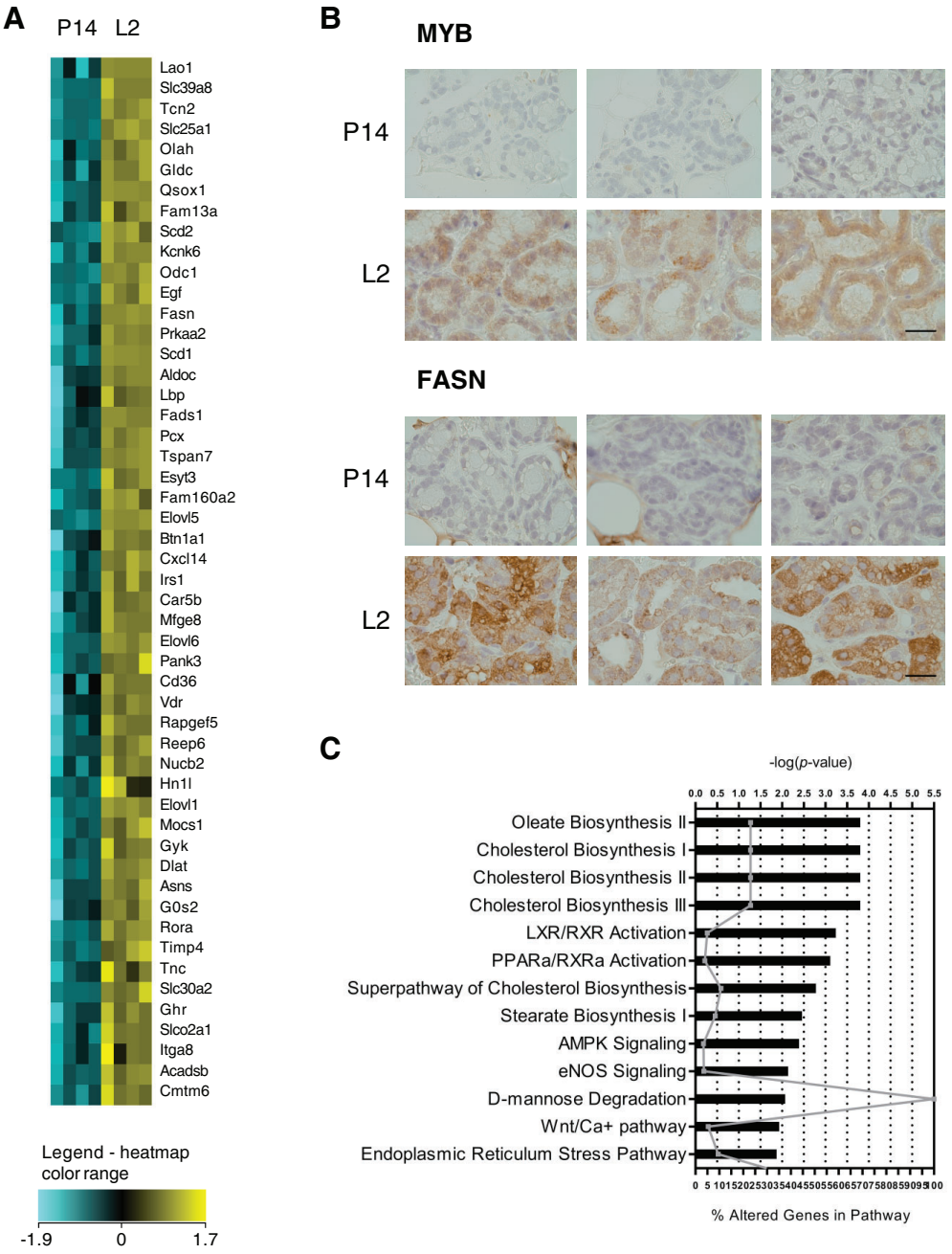

Fig. 2. The decline of miR-150-5p at L2 coincides with increased predicted lipogenic mRNA targets.
(A) Affymetrix GeneChip Mouse Gene 1.0 ST array heatmap depicting normalized signal values of miR-150-5p predicted targets from CD1 mouse MECs at P14 and L2 (four mice per time point). Significant mRNAs sorted from most increased in fold-change at the top to least increased at the bottom with a threefold cutoff due to space constraints. (B) IHC for validated target MYB and predicted target FASN at P14 versus L2 (three mice per time point). Scale bar: 20 µm. (C) Top 13 altered pathways based only on predicted miR-150-5p targets that were increased at L2 compared with P14, inverse to the decrease in miR-150-5p expression. Pathways were sorted in order of decreasing statistical significance (–log of *P*-value), represented by black bars with values indicated on the top axis. Gray line represents the percentage of altered genes in each pathway with values indicated on the bottom axis.

miR-150-5p revealed that lipid and cholesterol biosynthesis pathways at secretory activation were among the most significantly enhanced pathways correlated with the decline in miR-150-5p at L2 (Fig. 2C).

miR-150-5p plays a potentially different role at mid-pregnancy

ISH for miR-150 on C57BL/6 mouse MGs collected previously at days P5, P12, P17 and L1 (Spoelstra et al., 2006) indicated that miR-150-5p expression was low early in pregnancy (P5), increased mid to late pregnancy (between P12 and P17), and decreased just after secretory activation at L1 (Fig. S2A). To investigate a role for the rise in miR-150-5p at mid-pregnancy, we examined previously published time-course microarray data (GEO record GSE4222) (Rudolph et al., 2007) (Fig. S2B). Genes crucial for lactation, such as miR-150-5p predicted targets *Elovl5* and *Fads1*, are expressed at low levels until late pregnancy when they increase (Rudolph et al., 2007) coincident with the decline of miR-150-5p. Conversely, validated miR-150 targets *Egr2* (Bousquet et al., 2013) and *Myb* (Xiao et al., 2007) decreased at mid-pregnancy when miR-150 increased (Fig. S2B).

Constitutive expression of miR-150 in mammary epithelium throughout lactation leads to a severe lactation defect

The decrease in miRNAs such as miR-150-5p at L2 might allow for maximal and accurately timed expression of proteins important for secretory activation. To test this possibility, we used a transgenic mouse model designed to override the natural decline in miR-150 by constitutively expressing miR-150 in the mammary epithelium. Whey acidic protein-driven Cre recombinase (*WAP-Cre*$^{+}$) transgenic mice (Wagner et al., 1997) were crossed with *Rosa-26-flox-Stop-flox-miR-150*$^{fl/-}$ (*Stop-150*$^{fl/-}$) transgenic mice (Fig. 3A,B) created

Development (2016) 143, 4236-4248 doi:10.1242/dev.139642

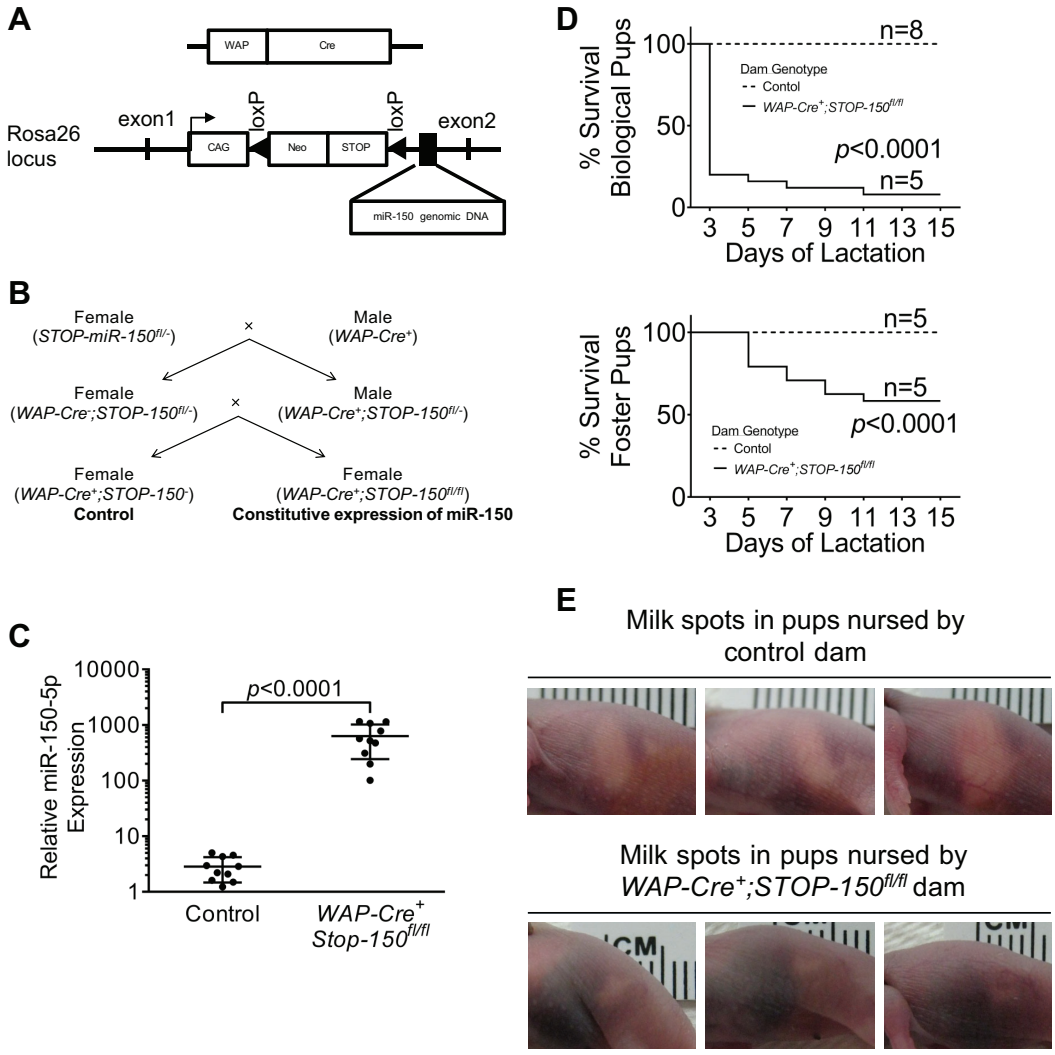

Fig. 3. Constitutive expression of miR-150 in mammary epithelium throughout lactation leads to a severe lactation defect. (A) Structures of the *WAP-Cre* and *Stop-150* transgenes. (B) Mice with constitutive expression of miR-150-5p in the mammary epithelium throughout lactation (genotype *WAP-Cre*$^{+}$*; Stop-150*$^{fl/fl}$) along with littermate controls (genotype *WAP-Cre*$^{+}$*; Stop-150*$^{-}$) were generated from breeding *STOP-150*$^{fl/-}$ mice with *WAP-Cre*$^{+}$ mice as indicated in the schematic. (C) L2 MECs from *WAP-Cre+; Stop-150*$^{fl/fl}$ mice showed a significant increase in miR-150-5p expression compared with MECs from controls. TaqMan qRT-PCR was used to quantify miR-150-5p expression normalized to RNAU6. Shown are mean±s.d., n=10, unpaired t-test. (D) Biological and fostered pups nursed by *WAP-Cre*$^{+}$*; Stop-150*$^{fl/fl}$ dams showed a significant decrease in survival compared with those nursed by control mice. Kaplan–Meier survival plots of biological and fostered pups nursed by the indicated dam genotypes, n=number of first-time litters included in the data, log-rank (Mantel–Cox) test. (E) Photos from representative surviving pups at L2, nursed by indicated genotypes, mm increments are shown on ruler behind each pup.

previously (Xiao et al., 2007). Sustained expression of mature miR-150-5p following secretory activation in L2 MECs from *WAP-Cre*$^{+}$*; Stop-150*$^{fl/fl}$ mice was confirmed by qRT-PCR (Fig. 3C). To determine if the miRNA processing machinery was potentially overburdened by constitutive synthesis of miR-150-p, miR-146b-5p, a miRNA that increased at L2 compared with P14 in wild-type mice (Fig. 1A), was analyzed and found to be unaffected by constitutive expression of miR-150 (Fig. S3).

Compared with offspring nursed by control dams (*WAP-Cre*$^{+}$*; Stop-150*$^{-}$), pups nursed by *WAP-Cre*$^{+}$*; Stop-150*$^{fl/fl}$ dams had significantly decreased survival by postnatal day (PND)3, which continued to diminish throughout lactation (Fig. 3D, top; P<0.0001). Surrogate litters from control dams confirmed the lactation defect persisted beyond PND3 as surrogate mortality was also significantly higher when nursed by *WAP-Cre*$^{+}$*; Stop-150*$^{fl/fl}$ dams relative to control dams (Fig. 3D, bottom; P<0.0001). Additional evidence of the lactation defect in dams constitutively expressing miR-150 was observed in the milk spots of surviving pups at PND2, which were notably smaller in pups nursed by *WAP-Cre*$^{+}$*; Stop-150*$^{fl/fl}$ dams (Fig. 3E) These data indicate constitutive expression of miR-150-5p in mammary epithelium results in a severe lactation deficiency with death of over 50% of offspring by PND3.

Constitutive expression of miR-150 reduced alveolar density at L2 and decreased multiple proteins including total STAT5B and phosphorylated STAT5

To understand lactation defects at the cellular level, histological MG sections from P18 and L2 were evaluated for morphological changes. MGs from *WAP-Cre*$^{+}$*; Stop-150*$^{fl/fl}$ mice had no difference in alveolar density as late into pregnancy as P18 when compared with that from control mice (Fig. 4A). Furthermore, IHC for the lipid droplet-binding protein adipophilin indicated that *WAP-Cre*$^{+}$*; Stop-150*$^{fl/fl}$ mice have equivalent lipid droplet size and abundance

Development (2016) 143, 4236-4248 doi:10.1242/dev.139642

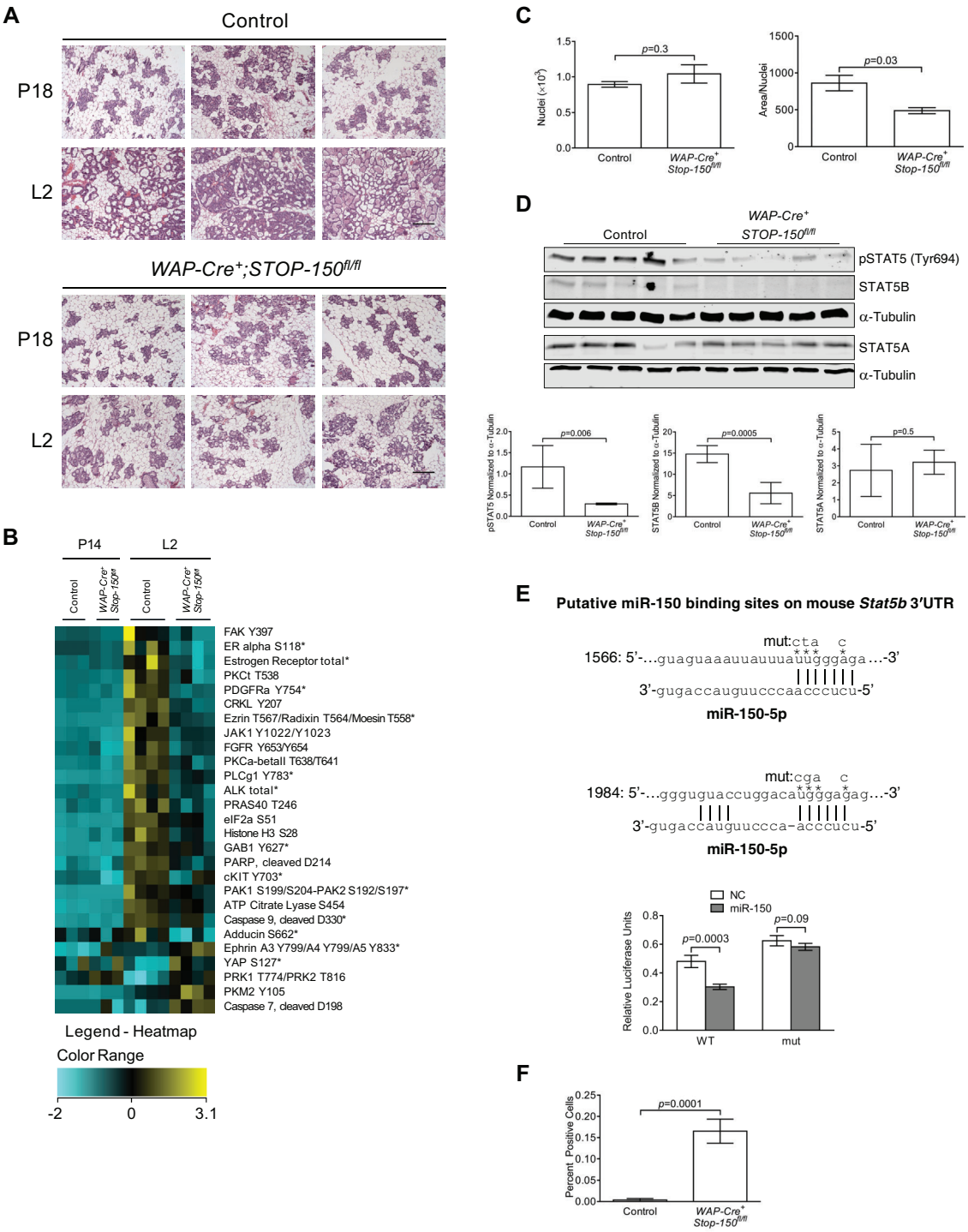

Fig. 4. Constitutive expression of miR-150 reduced alveolar density at L2 and decreased multiple proteins including total STAT5B and phosphorylated STAT5. (A) MGs from *WAP-Cre*$^{+}$*; Stop-150*$^{fl/fl}$ mice showed similar mammary alveoli density to control mice at P18, but reduced density at L2 compared with controls. H&E staining on MG sections from mice at P18 and L2 (three mice per time point and genotype). Scale bar: 200 µm. (B) Heatmap depicting reverse phase protein array normalized signal values of proteins significantly differentially expressed in P14 (three mice per genotype) and L2 (four mice per genotype) MECs from both genotypes. Significant protein differences at L2 (P<0.05) sorted by most decreased in fold-change at the top and most increased fold-change at the bottom. Asterisks indicate predicted targets of miR-150-5p based on TargetScan and RNA22. (C) Quantification of nuclei count on H&E staining on MG sections from mice at L2 (three mice per genotype). Shown are mean±s.d., unpaired *t*-test. (D) STAT5B expression and STAT5 activation were impaired in L2 MECs from *WAP-Cre*$^{+}$*; Stop-150*$^{fl/fl}$ mice compared with controls. Immunoblot analysis of MEC lysate using antibodies against indicated proteins and α-tubulin as a loading control, five mice per genotype, quantification for pSTAT5 and STAT5B excludes lane 4 of the control samples. Shown are mean±s.d., unpaired *t*-test. (E) The predicted miR-150-5p target sites in positions 1566-1573 and 1984-1990 of mouse *Stat5b*-3′ UTR are shown (top). 4T-1 cells were co-transfected with scrambled negative control (NC) or miR-150-5p mimic (miR-150) together with pmirGLO *Stat5b*-3′ UTR-WT or *Stat5b*-3′ UTR-mut plasmids and a luciferase assay was performed (bottom). Shown are mean±s.d., n=4, unpaired *t*-test. A similar result was seen from three independent experiments. (F) MGs from *WAP-Cre*$^{+}$*; Stop-150*$^{fl/fl}$ mice showed a significant increase in cell death during early lactation compared with controls. Quantification of cleaved caspase 3 IHC on MGs from mice with indicated genotypes at lactation day 2 (five controls and four *WAP-Cre*$^{+}$*; Stop-150*$^{fl/fl}$ mice). Shown are mean±s.d., unpaired *t*-test.

Development (2016) 143, 4236-4248 doi:10.1242/dev.139642

at P18 (Fig. S4). In contrast, there was decreased alveolar density between genotypes at L2 (Fig. 4A).

Reverse phase protein array (RPPA) was used to examine a variety of total and phosphorylated signal transduction proteins in MEC lysates from control and *WAP-Cre*$^{+}$*; Stop-150*$^{fl/fl}$ mice at both P14 and L2 (Fig. 4B). The majority of proteins differentially expressed between genotypes, including the phosphorylated forms of JAK1 (Y1022/Y1023), FAK (also known as PTK2) (Y397), and ER-alpha (also known as ESR1) (S118), were decreased by constitutive expression of miR-150 only at L2 (Fig. 4B), but there was no significant effect on protein expression levels at P14 (Fig. 4B; Table S4).

To explore the cause of morphological changes observed in the bitransgenic mice at L2 (Fig. 4A), histological sections were quantified for nuclei count and area (Fig. 4C). Because there was no difference in nuclei count (Fig. 4C, left), but epithelial area normalized to nuclei count was significantly reduced (Fig. 4C, right; P=0.03), the difference in observed alveolar density is due to the epithelium in control mice becoming distended with milk, whereas epithelium in bitransgenic mice was much less distended.

Prolactin receptor (PRLR) signaling mediated through janus kinase 2 (JAK2) and signal transducer and activator of transcription 5 (STAT5) is essential for lactation (Rudolph et al., 2011). Both total STAT5B (a TargetScan-predicted target of miR-150-5p) and phospho-STAT5 were significantly reduced in L2 MECs from *WAP-Cre*$^{+}$*; Stop-150*$^{fl/fl}$ mice compared with controls (P=0.006 and P=0.005, respectively), but STAT5A protein was not affected (Fig. 4D). The ability of miR-150-5p to target the *Stat5b* 3′ untranslated region (UTR) was tested with a *Stat5b*-3′-UTR-luciferase reporter containing the predicted miR-150-5p binding sites (Fig. 4E). Co-transfection of miR-150-5p mimic with plasmid containing the wild-type sequences of the two predicted miR-150-5p binding sites resulted in a significant decrease in reporter activity, but not co-transfection with the *Stat5b*-3′ UTR-mut plasmid in which residues crucial to miR-150-5p binding were mutated at both sites (Fig. 4E; P=0.0003 and P=0.09, respectively). This demonstrated that mouse *Stat5b* is a bona fide target of miR-150-5p. Importantly, activated and total janus kinase 2 (JAK2) were similar in L2 MECs from *WAP-Cre*$^{+}$*; Stop-150*$^{fl/fl}$ mice compared with controls, suggesting there was normal PRLR activation upstream of STAT5 (Fig. S5). Thus, our data indicate that targeted reduction of STAT5B, resulting from constitutive expression of miR-150, might impair secretory activation specifically through reduced total STAT5 activity.

Because STAT5 contributes to survival of differentiated mammary epithelium (Cui et al., 2004), cell death was investigated by IHC to detect cleaved caspase 3 (CC3) in sections of L2 MGs from *WAP-Cre*$^{+}$*; Stop-150*$^{fl/fl}$ mice. Although less than 0.2% of MECs were CC3-positive, CC3 staining was significantly higher in MGs from *WAP-Cre*$^{+}$*; Stop-150*$^{fl/fl}$ mice compared with controls (Fig. 4F; P=0.0001), indicating that constitutive expression of miR-150 caused some increased cell death in mammary epithelium.

Lipid and cholesterol synthesis transcripts are preferentially reduced by constitutive expression of miR-150

Global mRNA profiling identified significant gene expression changes due to constitutive expression of miR-150 in MECs (analyzed data in Table S5). In agreement with the bioinformatic predictions shown in Fig. 2C, more than half of the genes involved in lipid and cholesterol synthesis had a ≥twofold decrease due to constitutive expression of miR-150 at L2 (Fig. 5). Of the 22 listed lipid and cholesterol synthesis genes with a ≥twofold decrease, all but two are predicted to be direct targets of miR-150 (TargetScan and RNA22). Notably, these predicted targets include the primary enzymes of the *de novo* fatty acid synthesis pathway, including ATP citrate lyase (*Acly*) (Linn and Srere, 1979), acetyl-CoA carboxylase (*Acaca*, both isoforms) (Harada et al., 2007), *Fasn* (Smith et al., 2003), and thyroid hormone responsive protein spot 14 (*Thrsp*) (Rudolph et al., 2014). Further, mitochondrial citrate transporter (*Slc25a1*), required to shuttle substrate into the *de novo* fatty acid synthesis pathway (Kaplan et al., 1993) also decreased. Transcripts of genes that modify fatty acids including stearoyl-CoA desaturase 1 (*Scd1*), fatty acid elongases (*Elovl5* and *Elovl6*), and the fatty acid desaturase (*Fads1*) were also decreased by miR-150 expression.

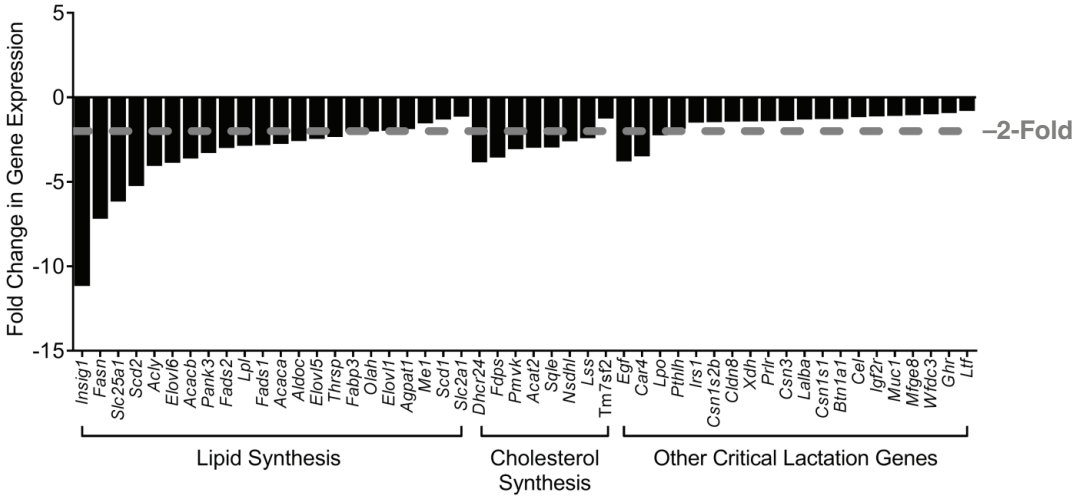

Fig. 5. Lipid and cholesterol synthesis transcripts are preferentially reduced by constitutive expression of miR-150. Negative fold-change values for genes crucial to lactation were calculated from the Affymetrix GeneChip Mouse Transcriptome Array 1.0 microarray performed on RNA from L2 MECs of both genotypes (control and *WAP-Cre*$^{+}$*; Stop-150*$^{fl/fl}$), n=3. Genes within each category are sorted from greatest to smallest fold-decrease based on the Mouse Transcriptome Array. Transcripts of all genes shown normally increase by twofold or greater at L2 compared with P14 based on the Mouse Gene 1.0 ST array. Dotted line represents twofold decrease.

Development (2016) 143, 4236-4248 doi:10.1242/dev.139642

FASN, ACACA and OLAH, all involved in *de novo* lipid synthesis, are suppressed by constitutive expression of miR-150

FASN is absolutely essential in mammals to synthesize *de novo* fatty acids from acetyl-CoA and malonyl-CoA substrates (Smith et al., 2003). Because *Fasn* and *Acaca*, which encodes the enzyme supplying substrate to FASN, were decreased significantly at L2 in mice with constitutively expressed miR-150 (Fig. 5), protein levels were evaluated by immunoblot and IHC. Immunoblot analysis indicated an ∼85% (P=0.0001) suppression of FASN protein in L2 MEC lysates from *WAP-Cre*$^{+}$*; Stop-150*$^{fl/fl}$ mice compared with control MECs (Fig. 6A). In addition, IHC analysis revealed that whereas FASN levels in the epithelium of control mice increased dramatically from P14 to L2 (Fig. 6B, top), FASN was inhibited at L2 in *WAP-Cre*$^{+}$*; Stop-150*$^{fl/fl}$ mammary epithelium, but not in mammary adipose (Fig. 6B, bottom). This result indicates epithelial cell-specific expression of exogenous miR-150 coincided with MEC-specific suppression of FASN. The ability of miR-150-5p to target a predicted site in the *Fasn* 3′ UTR was tested using a *Fasn*-3′-UTR-luciferase reporter assay (Fig. 6C). Co-transfection of miR-150 mimic resulted in a significant decrease in reporter activity with reporter containing the wild-type *Fasn* 3′ UTR miR-150-5p target site, but not with the *Fasn*-3′-UTR-mut plasmid, in which residues crucial to miR-150-5p binding were mutated (Fig. 6C). This demonstrated that mouse *Fasn* is a bona fide target of miR-150-5p. Whereas ACACA (a RNA22-predicted target of miR-150-5p) increased at the protein level between P14 and L2 in MECs of control mice (Fig. 7A, top), epithelial expression of ACACA was significantly decreased in L2 glands from *WAP-Cre*$^{+}$*; Stop-150*$^{fl/fl}$ mice as shown by immunoblot analysis of MECs (∼80% decrease; Fig. 7B) and IHC (Fig. 7A, bottom). Although the transcript for oleoyl-ACP hydrolase (*Olah*) did not decrease with constitutive expression of miR-150 (Fig. 5), *Olah* is a predicted target of miR-150-5p (TargetScan) that is essential for synthesis of medium chain fatty acids (MCFA) in MECs (Smith, 1980). OLAH protein was suppressed by ∼60% in L2 MECs from *WAP-Cre*$^{+}$*; Stop-150*$^{fl/fl}$ mice compared with control mice as quantified by immunoblot (Fig. 7C). Collectively, these results demonstrate that expression of multiple *de novo* fatty acid synthesis pathway components are suppressed by constitutive expression of miR-150.

Constitutive expression of miR-150 results in reduced *de novo* fatty acid synthesis

To test the functional effects of the reduced levels of multiple proteins in the *de novo* fatty acid synthesis pathway, amounts of fatty acids were quantified from MECs using gas chromatography-mass spectrometry (GC-MS). MCFAs are known to be exclusively synthesized by the *de novo* pathway in MECs, owing to MEC-specific expression of OLAH (Smith, 1980). Quantitative lipid mass spectrometry revealed a significant reduction in MCFA, including 10:0, 12:0, and 14:0 (Fig. 8A; P<0.05, P<0.01 and P<0.05, respectively) as well as their sum (inset) in MECs that constitutively express miR-150 compared with control MECs. Furthermore, 16:0, which can originate from either MEC *de novo* synthesis or be taken up from the serum, was also significantly decreased in MECs from

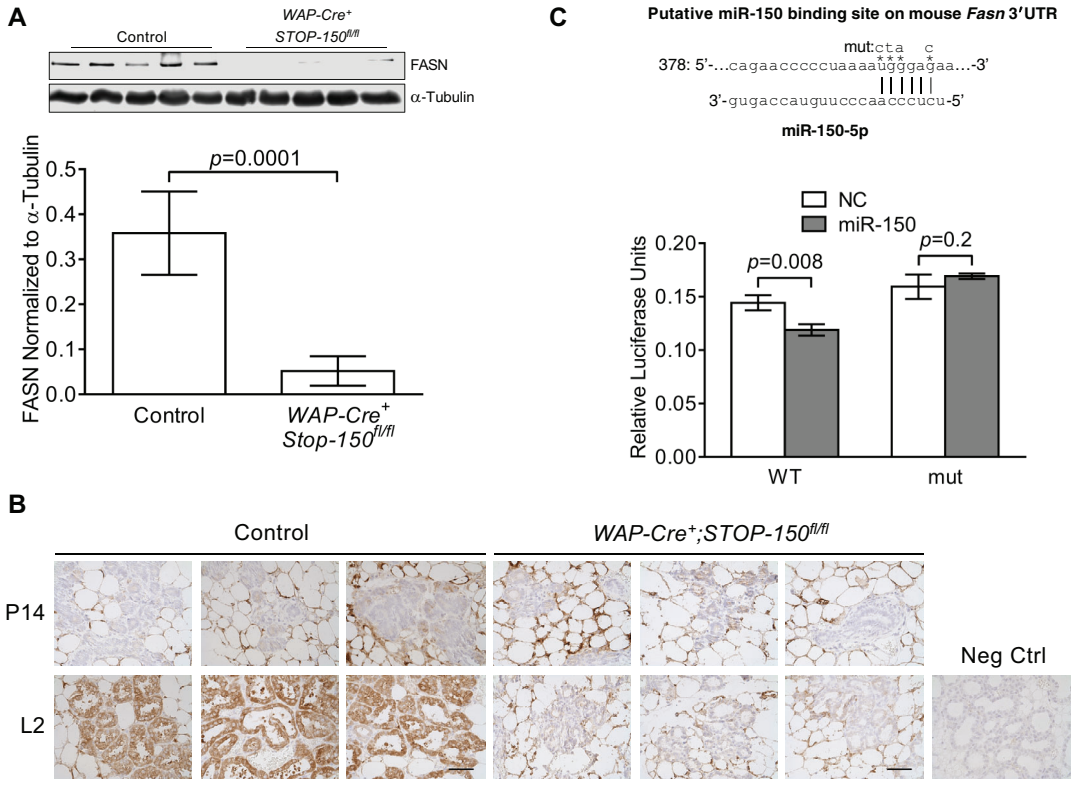

Fig. 6. Mouse FASN is a direct target of miR-150-5p. (A,B) FASN protein was significantly decreased in L2 MECs from *WAP-Cre*$^{+}$*; Stop-150*$^{fl/fl}$ mice compared with controls. (A) Immunoblot analysis using antibodies against FASN, and α-tubulin as a loading control, five mice per genotype, quantification of immunoblot using Image Studio (bottom). Shown are mean±s.d., unpaired *t*-test. (B) IHC for FASN from mice at P14 and L2 (three mice per indicated genotype) and negative control (no primary antibody). Scale bar: 50 µm. (C) The predicted miR-150-5p target site in position 378-384 of mouse *Fasn*-3′ UTR is shown (top). 4T-1 cells were co-transfected with scrambled negative control (NC) or miR-150-5p mimic (miR-150) together with pmirGLO *Fasn*-3′ UTR-WT or *Fasn*-3′ UTR-mut plasmids and a luciferase assay performed (bottom). Shown are mean±s.d., n=3, unpaired *t*-test. A similar result was seen from three independent experiments.

Development (2016) 143, 4236-4248 doi:10.1242/dev.139642

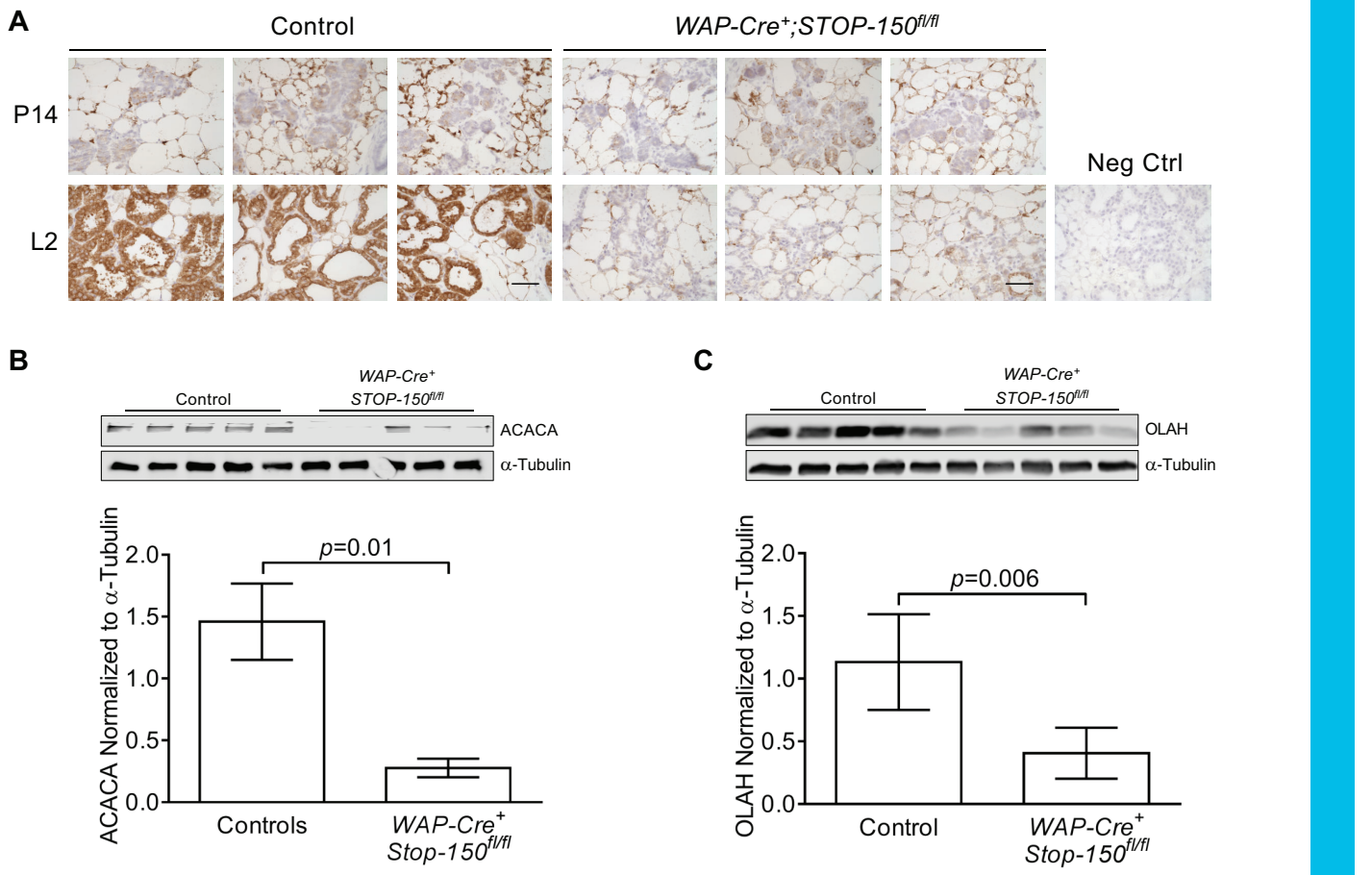

Fig. 7. ACACA and OLAH, both involved in lipid synthesis, are also suppressed by constitutive expression of miR-150. ACACA and OLAH protein were significantly decreased in L2 MECs from *WAP-Cre*$^{+}$*; Stop-150*$^{fl/fl}$ mice compared with controls. (A) IHC for ACACA in MGs from mice at P14 and L2 (three mice per indicated genotype) and negative control (no primary antibody). Scale bar: 50 µm. (B,C) Immunoblot analysis of MEC lysate using antibodies against ACACA, OLAH, and α-tubulin as a loading control, five mice per genotype, quantification of immunoblot was performed using Image Studio (bottom). Quantification excludes the third-to-last lane of the *WAP-Cre*$^{+}$*; Stop-150*$^{fl/fl}$ samples in B. Shown are mean±s.d., unpaired *t*-test.

mice with constitutive expression of miR-150 compared with controls (Fig. 8A; $P<0.05$). Production of 18:0 in MECs can result from elongation of 16:0 and was also significantly reduced in MECs from mice with constitutive expression of miR-150 compared with control mice (Fig. 8A; $P<0.01$). Although the classes of monounsaturated fatty acids (MUFA) and polyunsaturated fatty acids (PUFA) were unchanged (Fig. 8B) in MECs from mice with constitutive expression of miR-150 compared with control mice, a significant increase in 22:4 n-6 ($P<0.01$) and a nearly significant increase in 22:5 n-3 ($P=0.052$) were observed (Fig. 8C). Furthermore, fatty acids known to be taken up by MECs exclusively from dietary sources were not different (Fig. 8D). Collectively, quantitative GC-MS exposed the significant suppression of *de novo* synthesized fatty acids, further indicating that miR-150-5p profoundly modulates this enzymatic pathway *in vivo*.

DISCUSSION

We identified a variety of miRNA in differentiated MECs, including miR-150-5p, that decrease at the transition from pregnancy to lactation. These decreases in miRNA occur reciprocally with multiple mRNA increases in MECs, suggesting that the decline in miRNA could serve to relieve repression of mRNAs crucial for secretory activation and effective lactation. To test this hypothesis we constitutively expressed miR-150-5p, the miRNA with the highest fold-decrease between L2 versus P14, to override its natural decline. Our prediction was that transcripts targeted by miR-150-5p, which would normally be translated when this miRNA declines, would continue to be translationally inhibited with forced miR-150 expression, resulting in impaired lactation. Indeed, constitutive expression of miR-150-5p suppresses transcripts that code for proteins important for *de novo* fatty acid synthesis (FASN, ACACA and OLAH) and cell survival (STAT5B) in mammary epithelium. Our findings demonstrate that miR-150-5p directly targets the 3′ UTRs of mouse *Fasn* and *Stat5b* at predicted binding sites, suggesting regulatory control of two pathways crucial for lactation. Cumulatively, when miR-150-5p is constitutively expressed, synthesis of *de novo* fatty acids is dramatically reduced, which affects fatty acid content and results in severe lactation deficit and high pup mortality.

Consistent with miR-150-5p targeting *Stat5b* (Fig. 4D,E), constitutive expression of miR-150 results in a phenotype similar to that of *Stat5b* knockout mice (Udy et al., 1997). *Stat5b* knockout mice had impaired milk production and a high incidence of perinatal pup death. As STAT5 activity is important for survival of differentiated MECs (Cui et al., 2004), it is possible that targeted reduction of STAT5B protein by constitutive expression of miR-150 and consequent decreased total STAT5 activity contributed to decreased MEC survival at lactation. Reduced alveolar density

Development (2016) 143, 4236-4248 doi:10.1242/dev.139642

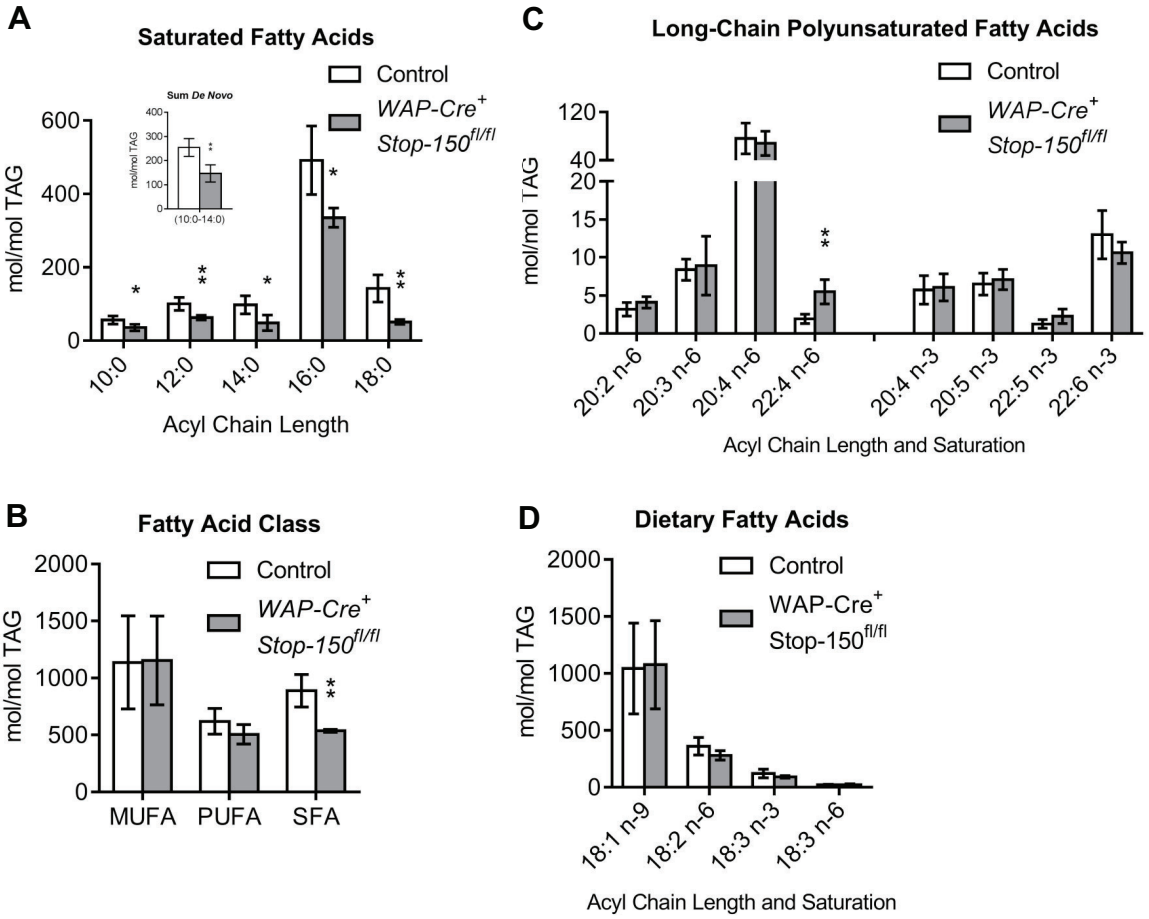

Fig. 8. Constitutive expression of miR-150 results in reduced *de novo* fatty acid synthesis. Total lipids were extracted from L2 MECs from mice of both genotypes and quantified by gas-chromatography mass spectrometry. (A) Synthesis of saturated fatty acids (SFA) was reduced overall in L2 MECs from *WAP-Cre*$^{+}$*; Stop-150*$^{fl/fl}$ mice compared with controls. The sum of the *de novo* synthesized fatty acids (10:0-14:0, P=0.003) shown in the inset. (B,C) MUFA and PUFA fatty acid classes were unchanged by constitutive expression of miR-150 (B), but long-chain PUFA 22:4 n-6 was significantly increased (P=0.002) (C). (D) Dietary fatty acids in L2 MECs were unaffected by constitutive expression of miR-150. Shown are mean±s.d., n=5 for controls, n=3 for *WAP-Cre*$^{+}$*; Stop-150*$^{fl/fl}$, unpaired *t*-test. *P<0.05, **P<0.01.

(Fig. 4A,C) and a slight increase in cleaved caspase 3 in L2 MGs with constitutive expression of miR-150 (Fig. 4F) were consistent with this theory. Constitutive expression of miR-150 does not alter signaling upstream of STAT5B as no differences were observed in activation of JAK2, a key mediator of PRLR signaling (Fig. S5, Table S4). *Prlr* mRNA was not suppressed by constitutive expression of miR-150 (Fig. 5). Suppression of STAT5B had no effect on the transcripts encoding β-casein and whey acidic protein (WAP) (Fig. S5), likely because STAT5A, activated during secretory activation (Nevalainen et al., 2002), was not affected by constitutive expression of miR-150 (Fig. 4D). In contrast, suppression of both milk protein and lipogenic genes does occur when both STAT5A and STAT5B are repressed via inhibition of pituitary prolactin secretion (Rudolph et al., 2011; Naylor et al., 2005), or dominant-negative prolactin mimetic (Naylor et al., 2005).

We found that constitutive expression of miR-150-5p suppressed lipid synthesis mRNAs at secretory activation (Fig. 5). It has been suggested that lipogenic gene induction is mediated in part by STAT5 activity (Rudolph et al., 2011). Therefore, it is possible that downregulation of STAT5B and total STAT5 activity by miR-150 contributes to suppression of lipogenic genes at the transcriptional level. However, our data strongly support an additional layer of miR-150-5p-mediated post-transcriptional control of multiple enzymes essential for *de novo* fatty acid synthesis such as FASN, ACACA and OLAH (Figs 6 and 7).

FASN synthesizes all *de novo* fatty acids (Smith et al., 2003), ACACA is the primary rate-limiting enzyme in the *de novo* pathway responsible for supplying malonyl-CoA substrate to FASN (Harada et al., 2007), and OLAH releases the growing fatty acid chain specifically for medium chain fatty acids (MCFA) (Smith, 1980). Interestingly, numerous other predicted targets in this same pathway were suppressed twofold or more by constitutive expression of miR-150 (Fig. 5) including *Thrsp*, required for MCFA synthesis in MECs (Rudolph et al., 2014), *Acly*, responsible for synthesis of the substrate acetyl-CoA used for *de novo* fatty acid synthesis (Linn and Srere, 1979), and *Slc25a1*, which shuttles substrate into the *de novo* fatty acid synthesis pathway (Kaplan et al., 1993). These targets, like FASN, might be suppressed even more strongly at the protein level. Likely due to suppression of multiple key components of this pathway, MECs from *WAP-Cre*$^{+}$*; Stop-150*$^{fl/fl}$ mice had a profound deficit in saturated fatty acids (Fig. 8A), with notably less *de novo* fatty acid synthesized MCFA per mole of triacylglyceride (TAG), including 10:0, 12:0 and 14:0.

Fasn knockout mice (*Fasn* KO) also exhibit a lactation defect characterized by decreased pup weight, increased pup mortality, and milk containing significantly less 14:0, 16:0, 18:0, and overall fatty

Development (2016) 143, 4236-4248 doi:10.1242/dev.139642

acids compared with controls (Suburu et al., 2014). However, constitutive expression of miR-150 additionally affected the MCFA10:0 and 12:0 (Fig. 8A) and demonstrated a more dramatic effect on pup mortality. This broader reduction in MCFA can be attributed to suppression of the aforementioned additional key enzymes involved in *de novo* fatty acid synthesis. Furthermore, reduction in 18:0 (Fig. 8A) is also consistent with the observed decrease in its synthetic precursor, 16:0 (Fig. 8A), plus decreases in mRNA for fatty acid elongases, such as *Elovl6* (Fig. 5) that catalyze the synthesis of 18:0 from 16:0 (Moon et al., 2001). Despite decreased 18:0 substrate levels (Fig. 8A) and the observed reductions of *Scd1* and *Scd2* mRNA (Fig. 5), their product, 18:1 n-9, remained unaffected, likely due to the high quantity of 18:1 n-9 in our rodent diet. Thus, constitutive expression of miR-150 results in broader defects of milk fat composition than the *Fasn* KO, affecting both MCFA and long chain fatty acids.

It is likely that functional redundancies evolved such that multiple miRNAs, including miR-150, control lactation. For example, at least six other miRNAs that decline precipitously at secretory activation are predicted to target *Fasn*, including miR-342-3p, miR-361-5p, miR-425-5p, miR-17-3p, miR-15b-5p and miR-532-5p (Table S3). Functional overlap is also evident in miRNAs predicted to target transcripts of milk protein genes. For example, lactotransferrin (*Ltf*), is predicted to be targeted by six miRNAs significantly downregulated just prior to lactation, two of which are part of the miR-17/92 cluster (Table S6). Such redundancy could explain why knockout of the miR-17/92 cluster did not affect mammary development (Feuermann et al., 2012). Redundant function of miRNAs likely evolved as compensatory mechanisms for a process as crucial to mammalian survival as lactation. Consequently, forced expression to override the natural decrease in a miRNA might be a more effective method to evaluate the contribution of a specific miRNA to MG development than a knockout approach.

Interestingly, the initial rise in miR-150 at mid-pregnancy coincides with a decrease in direct targets of miR-150 such as *Myb* and *Egr2* (Fig. S2B) that encode proteins associated with proliferation (Miao et al., 2011; Liu et al., 2008), and these transcripts peak with proliferation of mammary epithelial cells (Traurig, 1967). Proliferative expansion precedes differentiation and the increase in miR-150-5p at mid-pregnancy might serve to halt proliferation, whereas its decline prior to secretory activation seems to serve an entirely different purpose, as described in this manuscript. Our RPPA data demonstrates that proteins affected by constitutive miR-150 at L2 are not affected by miR-150 at P14 (Fig. 4B). These are exciting examples of how the targets of a given miRNA might differ depending on the transcriptional drivers of mRNAs and what genes are actively being transcribed at particular stages of development – proliferative expansion, differentiation or secretory activation in the mammary gland.

We speculate that progesterone (P4) (in the additional context of high estrogen during pregnancy) could be a likely candidate for regulating miR-150 via the progesterone receptor, as P4 increases at mid-pregnancy when miR-150 increases, then drops precipitously in mice just prior to parturition when miR-150 declines.

Herein, we describe the effects of preventing the natural decline of a miRNA, miR-150, between late pregnancy and lactation. Our data support the hypothesis that a precipitous decline in a program of miRNAs, such as miR-150, provides a level of post-transcriptional control to fine-tune expression of specific proteins essential for the survival and function of differentiated MECs to achieve successful lactation.

MATERIALS AND METHODS

Mice

CD1 background mice were purchased from Taconic (Germantown, NY). *Stop-150$^{fl/fl}$* in C57BL/6 background were kindly provided by Changchun Xiao, The Scripps Research Institute (Xiao et al., 2007). *WAP-Cre^{+}* transgenic mice in FVB were originally generated as described (Wagner et al., 1997). At 8 weeks old, control females (*WAP-Cre^{+}; Stop-150^{-}*) or bitransgenic females with constitutive expression of miR-150 at late pregnancy and throughout lactation (*WAP-Cre^{+}; Stop-150$^{fl/fl}$*) were impregnated by wild-type males. P1 was identified as the first day a post-coital plug was observed. L1 was identified as the first day litters were present. MGs were harvested from dams at P14, P18 and L2. Pup survival data was collected from PND3 and every other day through lactation day 15 for first litters only. Initial litter size was defined as the total number of pups present at PND3. In fostering experiments, only litters born to control dams within 1 day of the biological litter were used as foster litters starting at PND3. All animal procedures were approved by the Institutional Animal Care and Use Committee of the University of Colorado Anschutz Medical Campus.

MEC isolation

Adipose-depleted mouse MECs were isolated from the upper inguinal MGs as described (Rudolph et al., 2009) with modifications (see supplementary Material and Methods).

RNA isolation

Total RNA was isolated from MECs using Trizol solution (Thermo Fisher Scientific, Waltham, MA, USA) and purified by Qiagen miRNA columns (Qiagen, Venlo, Netherlands). RNA concentration and purity were assessed in Applied Biosytems Bioanalyzer 2100 (Thermo Fisher Scientific).

Microarray hybridization

A 1 µg aliquot of total RNA from each sample was labeled with FlashTag Biotin RNA Labeling kit (Genisphere, Hatfield, PA, USA) and hybridized onto GeneChip Mouse Gene 1.0 ST, GeneChip miRNA 1.0 ST, and GeneChip Mouse Transcriptome Array 1.0 (Affymetrix, Santa Clara, CA, USA) according to the manufacturer's recommendations and performed in the University of Colorado Cancer Center Microarray Core Facility. The raw data for all three arrays are available at http://www.ncbi.nlm.nih.gov/geo under series records GSE87584 and GSE80666.

MicroRNA microarray data analysis

Data were extracted from the images, quantile normalized, summarized (median polish) and $\log_2$-transformed with miRNA QC tool software (Affymetrix). Data from mouse miRNAs were imported into GeneSpring GX10 (Agilent Technologies, Santa Clara, CA, USA) by creating a custom miRNA experiment, and differentially expressed miRNAs were identified using unpaired *t*-test. The *P*-values were corrected by multiple testing using Benjamini–Hochberg False Discovery Rate (BH-FDR). A 5% FDR cut-off was chosen to identify differentially expressed probe sets.

Gene expression data analysis

Affymetrix CEL files from all samples were loaded on to Genespring GX10. Signal intensities for all probe sets were obtained using Robust Multichip Averaging summarization algorithm, involving three steps – background correction, quantile normalization and probe summarization (median polish). Quality control was performed by principal component analysis to identify outliers. Differentially expressed probe sets between P14 and L2 were identified by performing an unpaired *t*-test to obtain raw *P*-values, which were subsequently corrected by multiple testing using the BH-FDR method. A 5% FDR cut-off was chosen to identify differentially expressed probe sets.

Quantitative reverse transcription polymerase chain reaction (qRT-PCR)

cDNA was synthesized using TaqMan MicroRNA Reverse Transcription kit (Thermo Fisher Scientific) and miRNA-specific RT primers as per manufacturer's recommendations. PCR for each miRNA was performed

Development (2016) 143, 4236-4248 doi:10.1242/dev.139642

using specific TaqMan MicroRNA probe and ABsolute Fast QPCR Low ROX mix (2×) (Thermo Fisher Scientific) or TaqMan Universal PCR Master Mix, no AmpErase UNG (2×) (Thermo Fisher Scientific). Quantification is described in supplementary Materials and Methods.

MicroRNA *in situ* hybridization

Lower thoracic glands were fixed in 10% neutral buffered formalin. Tissue processing and paraffin embedding were performed by the University of Colorado Denver Histology Shared Resource. Sections of MGs were analyzed by ISH as described in Cochrane et al., (2010). A hybridization temperature of 53°C and miRCURY LNA microRNA Detection Probes pre-labeled with double digoxigenin and complementary to mature miR-150-5p (CACTGGTACAAGGGTTGGGAGA) (Exiqon, Copenhagen, Denmark) were used.

Microscopy

Representative images of ISH, IHC and Hematoxylin and Eosin (H&E) slides were taken using an Olympus BX40 microscope (Center Valley, PA, USA) with a SPOT Insight Mosaic 4.2 camera and software (Diagnostic Instruments, Inc., Sterling Heights, MI, USA).

Canonical pathway analysis

Canonical pathway analysis was calculated using Ingenuity Pathway Analysis (Qiagen). Significance was calculated by Fisher's exact test right-tailed. The significance indicates the probability of association of altered molecules in the dataset with the pathway by random chance alone. The percent altered genes indicate the number of statistically significantly altered genes in the pathway divided by the total number of genes that make up that pathway.

microRNA target predictions

Targets of mmu-miR-150-5p were bioinformatically predicted using TargetScan Mouse v7.1, TargetScan Human v7.0 (Lewis et al., 2005), and RNA22 v2.0 (Miranda et al., 2006).

Immunohistochemistry

Sections of paraffin-embedded MGs were cut at 4 µm and deparaffinized in xylene, rehydrated with a series of graded ethanols, and subjected to heat-induced epitope retrieval in 10 mM citrate buffer, pH 6.0. Endogenous peroxidase was blocked, and slides were treated with 10% normal goat serum. Antibodies and detection methods are described in supplementary Materials and Methods. For CC3 staining, three separate 100× fields of each slide were analyzed with ImageJ (National Institutes of Health, Bethesda, MD, USA). Color threshold was adjusted manually; Red Green Blue (RGB) for positive-staining nuclei, and Hue Saturation Brightness (HSB) for total nuclei. RGB area was divided by HSB area to calculate percent positive CC3 cells.

H&E staining

H&E stains were purchased from Anatech (Battle Creek, MI, USA) and used per the manufacturer's instructions. Three separate 100× fields of each slide were analyzed. Nuclei were counted manually for each field. Alveolar pixel area was quantified using ImageJ by first subtracting non-epithelial tissue then adjusting a color threshold using HSB color space to include total epithelium. Nuclear density was calculated by dividing nuclei counts with the HSB area.

Reverse phase protein array

RPPA printing and analysis of MEC samples was conducted as previously described (Wulfkuhle et al., 2012, 2008; Sheehan et al., 2005). Before use for RPPA analysis, antibody specificity was confirmed by immunoblot and analysis, as previously described (Sheehan et al., 2005).

Immunoblot

Protein from each MEC sample (20 µg) was resolved by polyacrylamide gel electrophoresis and transferred to Immobilon-FL membranes (Millipore Continental Water Systems, Bedford, MA, USA). The membranes were blocked with 5% milk in PBS, probed with primary antibodies overnight at 4°C, washed and incubated with appropriate Alexa Fluor secondary antibody (Thermo Fisher Scientific) (see supplementary Materials and Methods section for details of antibodies). Protein was detected using an Odyssey infrared imager (LI-COR Biosciences, Lincoln, NE, USA).

Construction of *Fasn* and *Stat5b*-3′ UTR-luciferase reporters and luciferase reporter assay

The 3′ UTR DNA fragments of mouse *Fasn* (1896 bp, NM_007988) and *Stat5b* (2518 bp, NM_001113563) containing the putative miR-150-5p target sites were amplified by PCR from mouse genomic DNA (primers described in supplementary Materials and Methods) and cloned into the *Sac*I- and *Xho*I-digested pmirGLO vector downstream of the firefly luciferase cDNA sequence (Promega), resulting in the generation of *Fasn*-3′-UTR-luc and *Stat5b*-3′-UTR-luc plasmids. These plasmids were used as a template to generate DNA fragments with mutated miR-150-5p targeting sites (*Fasn*-3′-UTR-mut, *Stat5b*-3′-UTR-luc-mut) by using mutated oligos described in the supplementary Materials and Methods. DNA sequencing verified the sequence of both plasmids.

Murine mammary tumor 4T-1 cells were plated at 1×10^5 cells per well in a 24-well plate. The next day, cells were co-transfected with 50 nM of control RNA or miR-150 mimic (Ambion, Austin, TX, USA) together with 0.5 µg of aforementioned pmirGLO plasmids containing wild-type or mutated putative target sites using Lipofectamine 2000 (Thermo Fisher Scientific). Cells were lysed 48 h later and the dual-luciferase reporter assay system (Promega) was used to measure luciferase activity according to manufacturer's instructions.

Total lipid extraction

Because of the low milk yield from *WAP-Cre*$^{+}$*; Stop-150*$^{fl/fl}$ mammary glands compared with controls, even after administration of a bolus of oxytocin, lipids were extracted from isolated MECs. HPLC grade reagents were purchased from Sigma-Aldrich (St. Louis, MO, USA). Total lipid extraction was performed as previously described (Rudolph et al., 2014) with modifications described in supplementary Materials and Methods.

Quantification of MEC TAG

A 50 µl aliquot of isooctane suspended total lipid was taken to dryness under nitrogen gas, samples were resuspended in 200 µl dichloromethane that contained 15 µl of a 10% nonaethylene glycol monododecyl ether (Sigma-Aldrich) dissolved in dichloromethane (w/v). Samples were incubated for 5 min at 25°C and taken to dryness at 40°C for 25 min to ensure organic solvent was completely evaporated. Pellets contained triglyceride and nonionic surfactant complexes, to which 200 µl of reverse osmosis water was carefully added without mixing and incubated at 40°C for 10 min and followed by a gentle vortex. A standard regression curve was made using 80 nmol of tripalmitin (Sigma Aldrich) combined with 25 µl of 10% nonaethylene glycol monododecyl ether in dichloromethane (w/v), incubated and dried as above, suspended in 100 µl of reverse osmosis water, and dilutions of 20, 10, 5, 2.5, 1.25, 0.625 and 0.3125 nmol tripalmitin were used. Total TAG from the organic fraction was quantified relative to known tripalmitin standard using a modified colorimetric assay (Van Veldhoven et al., 1997) and values are expressed as mM concentrations. Triglyceride Reagent and Free Glycerol Reagent Development were purchased from Sigma-Aldrich and diluted according to the manufacturer's instructions.

Gas chromatography-mass spectrometry

Blended stable isotope internal standards containing 100 ng each of [D]3-decanoic acid; [D]3-lauric acid; [D]3-myristic acid; 1,2,3,4-[^{13}C]4-palmitic acid; [D]3-stearic acid; [D]4-oleic acid; [D]8-arachidonic acid and [D]5-docosahexanoic acid [purchased from Sigma-Aldrich, Cambridge Isotopes (Andover, MA, USA) or Cayman Chemical Co. (Ann Arbor, MI, USA) with 99 atom % ^{13}C and 99 atom % D, respectively] were added to the volume of each sample representing 5 nmol of MEC TAG as quantified above. Samples were taken to dryness under N_2 gas, suspended in 0.5 ml 100%

Development (2016) 143, 4236-4248 doi:10.1242/dev.139642

methanol, and were saponified at 45°C for 1 h by adding 0.5 ml of 1M sodium hydroxide mixing at 20 min intervals. Samples were acidified with 0.525 ml of 1 M HCl, vortexed vigorously; fatty acids were extracted twice with 1.0 ml of isooctane, and taken to dryness under N_2 gas. Saponified fatty acids were derivatized at room temperature for 30 min by addition of 30 µl of 1% pentafluorobenzyl bromide in acetonitrile and 30 µl of 1% N,N-diisopropylethylamine in acetonitrile according to Rudolph et al. (2014), after which the samples were taken to dryness under N_2 gas. The resulting pentafluorobenzyl fatty acid esters were suspended in 200 µl isooctane, vortexed, and transferred into vials for gas chromatography mass spectrometry.

Acknowledgements
We'd like to acknowledge Emanuel Petricoin and Julia Wulfkuhle at the Center for Applied Proteomics and Molecular Medicine at George Mason University for RPPA. The authors also acknowledge the Genomics and Microarray Core and other Shared Resources of Colorado's NIH/NCI Cancer Center Support Grant P30CA046934.

Competing interests
The authors declare no competing or financial interests.

Author contributions
Writing - original draft preparation: R.E.H., H.Gu., J.K.R. Writing - review and editing: R.E.H., M.C.R., P.R., N.S.S., M.A.G., H.Gu., J.K.R. Visualization: R.E.H. Investigation R.E.H., M.C.R., P.R., P.G.W., N.S.S., K.T.B., B.L.B., H.Ga., S.C., M.A.G., H.Gu. Formal analysis: R.E.H., M.C.R., P.R., N.S.S., M.C.N., S.M.A., M.A.G., H.Gu., J.K.R. Conceptualization: S.M.A., M.C.N., H.Gu., J.K.R.

Funding
This study was supported by the National Institutes of Health/Eunice Kennedy Shriver National Institute of Child Health and Human Development [Grant 5P01 HD038129-15 Functional Development of the Mammary Gland (PI, S.M.A.) Richer (PI Project 3)]; National Institutes of Health [Building Interdisciplinary Research Careers in Women's Health Scholarship K12 HD057022, Nutrition and Obesity Research Center Pilot Award 5P30DK048520-19]; and National Institutes of Health/National Center for Advancing Translational Sciences Colorado Clinical and Translational Science Institute [Grant TL1 TR001081]. This work was also supported in part by the startup fund from Wenzhou Medical University and the National Natural Science Foundation of China [Grant 81372826]. Lipid mass spectrometry was supported by National Institutes of Health/National Center for Advancing Translational Sciences Colorado Clinical and Translational Science Institute [Grant UL1 TR001082]. We acknowledge the use of the University of Colorado Cancer Center Shared Resources for microarray and tissue procurement and pathology supported by the National Institutes of Health/National Cancer Institute [Cancer Core Support Grant P30 CA046934]. Deposited in PMC for release after 12 months.

Data availability
The raw data for the three arrays used in the microarray hybridization study are available at Gene Expression Omnibus (GEO) (http://www.ncbi.nlm.nih.gov/geo) under accession numbers GSE87584 and GSE80666.

Supplementary information
Supplementary information available online at
http://dev.biologists.org/lookup/doi/10.1242/dev.139642.supplemental

References
Anderson, S. M., Rudolph, M. C., McManaman, J. L. and Neville, M. C. (2007). Key stages in mammary gland development. Secretory activation in the mammary gland: it's not just about milk protein synthesis! *Breast Cancer Res.* **9**, 204.

Avril-Sassen, S., Goldstein, L. D., Stingl, J., Blenkiron, C., Le Quesne, J., Spiteri, I., Karagavriilidou, K., Watson, C. J., Tavaré, S., Miska, E. A. et al. (2009). Characterisation of microRNA expression in post-natal mouse mammary gland development. *BMC Genomics* **10**, 548.

Bousquet, M., Zhuang, G., Meng, C., Ying, W., Cheruku, P. S., Shie, A. T., Wang, S., Ge, G., Wong, P., Wang, G. et al. (2013). miR-150 blocks MLL-AF9-associated leukemia through oncogene repression. *Mol. Cancer Res.* **11**, 912-922.

Cochrane, D. R., Cittelly, D. M., Howe, E. N., Spoelstra, N. S., Mckinsey, E. L., LaPara, K., Elias, A., Yee, D. and Richer, J. K. (2010). MicroRNAs link estrogen receptor alpha status and Dicer levels in breast cancer. *Horm. Cancer* **1**, 306-319.

Cui, Y., Riedlinger, G., Miyoshi, K., Tang, W., Li, C., Deng, C.-X., Robinson, G. W. and Hennighausen, L. (2004). Inactivation of Stat5 in mouse mammary epithelium during pregnancy reveals distinct functions in cell proliferation, survival, and differentiation. *Mol. Cell. Biol.* **24**, 8037-8047.

Feuermann, Y., Robinson, G. W., Zhu, B.-M., Kang, K., Raviv, N., Yamaji, D. and Hennighausen, L. (2012). The miR-17/92 cluster is targeted by STAT5 but dispensable for mammary development. *Genesis* **50**, 665-671.

Harada, N., Oda, Z., Hara, Y., Fujinami, K., Okawa, M., Ohbuchi, K., Yonemoto, M., Ikeda, Y., Ohwaki, K., Aragane, K. et al. (2007). Hepatic de novo lipogenesis is present in liver-specific ACC1-deficient mice. *Mol. Cell. Biol.* **27**, 1881-1888.

Kaplan, R. S., Mayor, J. A. and Wood, D. O. (1993). The mitochondrial tricarboxylate transport protein. cDNA cloning, primary structure, and comparison with other mitochondrial transport proteins. *J. Biol. Chem.* **268**, 13682-13690.

Lewis, B. P., Burge, C. B. and Bartel, D. P. (2005). Conserved seed pairing, often flanked by adenosines, indicates that thousands of human genes are microRNA targets. *Cell* **120**, 15-20.

Linn, T. C. and Srere, P. A. (1979). Identification of ATP citrate lyase as a phosphoprotein. *J. Biol. Chem.* **254**, 1691-1698.

Liu, C.-J., Liu, T.-Y., Kuo, L.-T., Cheng, H.-W., Chu, T.-H., Chang, K.-W. and Lin, S.-C. (2008). Differential gene expression signature between primary and metastatic head and neck squamous cell carcinoma. *J. Pathol.* **214**, 489-497.

Miao, R. Y., Drabsch, Y., Cross, R. S., Cheasley, D., Carpinteri, S., Pereira, L., Malaterre, J., Gonda, T. J., Anderson, R. L. and Ramsay, R. G. (2011). MYB is essential for mammary tumorigenesis. *Cancer Res.* **71**, 7029-7037.

Miranda, K. C., Huynh, T., Tay, Y., Ang, Y.-S., Tam, W.-L., Thomson, A. M., Lim, B. and Rigoutsos, I. (2006). A pattern-based method for the identification of microRNA binding sites and their corresponding heteroduplexes. *Cell* **126**, 1203-1217.

Moon, Y.-A., Shah, N. A., Mohapatra, S., Warrington, J. A. and Horton, J. D. (2001). Identification of a mammalian long chain fatty acyl elongase regulated by sterol regulatory element-binding proteins. *J. Biol. Chem.* **276**, 45358-45366.

Naylor, M. J., Oakes, S. R., Gardiner-Garden, M., Harris, J., Blazek, K., Ho, T. W. C., Li, F. C., Wynick, D., Walker, A. M. and Ormandy, C. J. (2005). Transcriptional changes underlying the secretory activation phase of mammary gland development. *Mol. Endocrinol.* **19**, 1868-1883.

Nevalainen, M. T., Xie, J., Bubendorf, L., Wagner, K.-U. and Rui, H. (2002). Basal activation of transcription factor signal transducer and activator of transcription (Stat5) in nonpregnant mouse and human breast epithelium. *Mol. Endocrinol.* **16**, 1108-1124.

Rudolph, M. C., McManaman, J. L., Hunter, L., Phang, T. and Neville, M. C. (2003). Functional development of the mammary gland: use of expression profiling and trajectory clustering to reveal changes in gene expression during pregnancy, lactation, and involution. *J. Mammary Gland Biol. Neoplasia* **8**, 287-307.

Rudolph, M. C., McManaman, J. L., Phang, T., Russell, T., Kominsky, D. J., Serkova, N. J., Stein, T., Anderson, S. M. and Neville, M. C. (2007). Metabolic regulation in the lactating mammary gland: a lipid synthesizing machine. *Physiol. Genomics* **28**, 323-336.

Rudolph, M. C., Wellberg, E. A. and Anderson, S. M. (2009). Adipose-depleted mammary epithelial cells and organoids. *J. Mammary Gland Biol. Neoplasia* **14**, 381-386.

Rudolph, M. C., Russell, T. D., Webb, P., Neville, M. C. and Anderson, S. M. (2011). Prolactin-mediated regulation of lipid biosynthesis genes in vivo in the lactating mammary epithelial cell. *Am. J. Physiol. Endocrinol. Metab.* **300**, E1059-E1068.

Rudolph, M. C., Wellberg, E. A., Lewis, A. S., Terrell, K. L., Merz, A. L., Maluf, N. K., Serkova, N. J. and Anderson, S. M. (2014). Thyroid hormone responsive protein Spot14 enhances catalysis of fatty acid synthase in lactating mammary epithelium. *J. Lipid Res.* **55**, 1052-1065.

Sheehan, K. M., Calvert, V. S., Kay, E. W., Lu, Y., Fishman, D., Espina, V., Aquino, J., Speer, R., Araujo, R., Mills, G. B. et al. (2005). Use of reverse phase protein microarrays and reference standard development for molecular network analysis of metastatic ovarian carcinoma. *Mol. Cell. Proteomics* **4**, 346-355.

Smith, S. (1980). Mechanism of chain length determination in biosynthesis of milk fatty acids. *J. Dairy Sci.* **63**, 337-352.

Smith, S., Witkowski, A. and Joshi, A. K. (2003). Structural and functional organization of the animal fatty acid synthase. *Prog. Lipid Res.* **42**, 289-317.

Spoelstra, N. S., Manning, N. G., Higashi, Y., Darling, D., Singh, M., Shroyer, K. R., Broaddus, R. R., Horwitz, K. B. and Richer, J. K. (2006). The transcription factor ZEB1 is aberrantly expressed in aggressive uterine cancers. *Cancer Res.* **66**, 3893-3902.

Suburu, J., Shi, L., Wu, J., Wang, S., Samuel, M., Thomas, M. J., Kock, N. D., Yang, G., Kridel, S. and Chen, Y. Q. (2014). Fatty acid synthase is required for mammary gland development and milk production during lactation. *Am. J. Physiol. Endocrinol. Metab.* **306**, E1132-E1143.

Traurig, H. (1967). Cell proliferation in the mammary gland during late pregnancy and lactation. *Anat. Rec.* **157**, 489-503.

Udy, G. B., Towers, R. P., Snell, R. G., Wilkins, R. J., Park, S.-H., Ram, P. A., Waxman, D. J. and Davey, H. W. (1997). Requirement of STAT5b for sexual dimorphism of body growth rates and liver gene expression. *Proc. Natl. Acad. Sci. USA* **94**, 7239-7244.

Development (2016) 143, 4236-4248 doi:10.1242/dev.139642

Van Veldhoven, P. P., Swinnen, J. V., Esquenet, M. and Verhoeven, G. (1997). Lipase-based quantitation of triacylglycerols in cellular lipid extracts: requirement for presence of detergent and prior separation by thin-layer chromatography. *Lipids* **32**, 1297-1300.

Wagner, K.-U., Wall, R. J., St-Onge, L., Gruss, P., Wynshaw-Boris, A., Garrett, L., Li, M., Furth, P. A. and Hennighausen, L. (1997). Cre-mediated gene deletion in the mammary gland. *Nucleic Acids Res.* **25**, 4323-4330.

Wulfkuhle, J. D., Speer, R., Pierobon, M., Laird, J., Espina, V., Deng, J., Mammano, E., Yang, S. X., Swain, S. M., Nitti, D. et al. (2008). Multiplexed cell signaling analysis of human breast cancer applications for personalized therapy. *J Proteome Res.* **7**, 1508-1517.

Wulfkuhle, J. D., Berg, D., Wolff, C., Langer, R., Tran, K., Illi, J., Espina, V., Pierobon, M., Deng, J., DeMichele, A. et al. (2012). Molecular analysis of HER2 signaling in human breast cancer by functional protein pathway activation mapping. *Clin. Cancer Res.* **18**, 6426-6435.

Xiao, C., Calado, D. P., Galler, G., Thai, T.-H., Patterson, H. C., Wang, J., Rajewsky, N., Bender, T. P. and Rajewsky, K. (2007). MiR-150 controls B cell differentiation by targeting the transcription factor c-Myb. *Cell* **131**, 146-159.

Supplemental Materials and Methods

MEC isolation

Modifications to the MEC isolation procedure as described (Rudolph et al., 2009) were made for MEC isolation of transgenic mice. Specifically, after removal of lymph nodes, the MGs were removed, minced, and digested with 1 mg/mL collagenase type 1 (Worthington Biochemical Corporation, LS004196) in Dulbecco's Modified Eagle Medium: Nutrient Mixture F-12 (HyClone, 11330-032), for 80 min in a 37°C rotor. Collagenase was then quenched with 0.5% fetal bovine serum, and the digested cell suspension was pelleted by centrifugation. Erythrocytes were then removed by successive washes of the cell pellet in Dulbecco's phosphate-buffered saline with calcium and magnesium (Hyclone SH30264.01) followed by 2-second centrifugations at 1500 rpm until pellet was no longer red. Cell pellets were then split into fractions for protein analysis, RNA isolation, and lipid extraction.

Quantitative reverse transcription polymerase chain reaction (qRT-PCR)

Quantification of miRNA was determined by calculating the relative copy number of each miRNA or the comparative threshold cycle (C_t) method. To estimate relative copy number, a standard curve was run using five four-fold dilutions of a P14 sample in duplicates. To calculate $2^{-\Delta\Delta Ct}$, the C_t values for RNAU6 were subtracted from C_t values of the miRNA to achieve the ΔC_t value. The ΔC_t of a control sample was then subtracted from each ΔC_t to achieve the relative miRNA levels ($\Delta\Delta C_t$). Fold change is calculated ($2^{-\Delta\Delta Ct}$). Statistical differences in miRNA expression between P14 and L2 samples were analysed by *t*-test.

Immunohistochemistry

Primary antibodies used were anti-FASN (Abcam ab22759, 1:8000, used for Fig. 2B and BD Biosciences 610962, Franklin Lakes, NJ, USA, 1:3,200, used for Fig. 6B), anti-MYB (Millipore 05-175, Billerica, MA, USA, 1:50), anti-adipophilin (Fitzgerald 20-AP002, Acton, MA, USA, 1:1600), anti-ACACA (Cell Signaling Technology 3676, Danvers, MA, USA, 1:1,600) and anti-CC3 (Cell Signaling Technology 9661, 1:1,600). Primary antibody detection was performed with either EnVision+ System-HRP labeled polymer secondary (Agilent Technologies K4001,K4003) or secondary antibody labeled with biotin (Dako/Agilent Technologies E0433, Carpinteria, CA,

1:500; Jackson Immuno Research, West Grove, PA, USA, 1:250) followed by incubation with streptavidin-HRP (Dako, 1:1000) and 3, 3′-diaminobenzidine (Dako) detection.

Immunoblot

The primary antibodies used were anti-pSTAT5 (Tyr694) (Cell Signaling Technology, 9351, 1:1000), anti-STAT5B (Millipore, 06-554, 1:1000), anti-STAT5A (Millipore, 06-968, 1:500), anti-whey acidic protein (WAP) (Santa Cruz, 398276, 1:300), anti-FASN (Cell Signaling Technology, 9363, 1:1000), anti-ACACA (Cell Signaling Technology, 3676, 1:1000), anti-OLAH (generous gift of Dr. Stuart Smith, Children's Hospital Oakland Research Institute, Oakland, CA, USA, 1:500), and anti-α-tubulin loading control (Sigma, T5168, 1:20,000). Secondary antibodies used were goat anti-mouse or rabbit Alexa Fluor 680® (Molecular probes, Grand Island, NY, USA)

Oligo primers for cloning of mouse 3′ UTR for Fasn

For *Fasn*-3′-UTR-WT: forward 5′-ATTGAGCTCACCTGCCGACCACCATGAAG-3′ and reverse 5′-CGGCTCGAGATTTCAGTCTTGTTCCACTCA-3′; For *Fasn*-3′-UTR-mut: forward 5′-CCCTAAAACTAGAGAAGCCATGTGGGGAAG-3′ and reverse 5′-CATGGCTTCTCTAGTTTTAGGGGGTTCTGG-3′.

Oligo primers for cloning of mouse 3′ UTR for Stat5b

For *Stat5b*-3′-UTR-WT site 1: forward 5′-GTAAATTATTTATTGGGAGATGAGTTTTTAAAAGCTGCTG-3′ and reverse 5′-CTCATCTCCCAATAAATAATTTACTACACAGGAGTTTG-3′; For *Stat5b*-3′-UTR-mut site 1: forward 5′-GTAAATTATTTACGAGGCGATGAGTTTTTAAAAGCTGCTG-3′ and reverse 5′-CTCATCGCCTCGTAAATAATTTACTACACAGGAGTTTG-3′; For *Stat5b*-3′-UTR-WT site 2: forward 5′-GTACCTGGACATGGGAGAGGTTTTTAACTGGAAAGTG-3′ and reverse 5′-GTTAAAAACCTCTCCCATGTCCAGGTACACCCTCAG-3′; For *Stat5b*-3′-UTR-mut site 2: forward 5′-GTACCTGGACACTAGACAGGTTTTTAACTGGAAAGTG-3′ and reverse 5′-GTTAAAAACCTGTCTAGTGTCCAGGTACACCCTCAG-3′.Detailed methods for generating *Fasn*-3′-UTR-mut and *Stat5b*-3′-UTR-mut plasmids are available upon request.

Total lipid extraction

Briefly, 7-20 mg of MEC pellet was suspended in 250 µL of 100 mM potassium phosphate buffer pH 7.2, mixed by inversion, acidified with 20 µL of 1 M HCl, 500 µL of 100% methanol was added, and samples were homogenized by rotor/stator. Lysates were cleared by centrifugation and supernatant transferred to glass tubes. Total lipids were extracted with 2 × 1 mL of isooctane/ethyl acetate 3:1 v/v and vortexed vigorously. The organic phase was collected and taken to dryness by evaporation under nitrogen gas at 40°C, and samples were resuspended in 250 µL of isooctane.

Quantification of MEC TAG and fatty acids

50 µL of isooctane suspended total lipid was taken to dryness under nitrogen gas, samples were resuspended in 200 µL dichloromethane that contained 15 µL of a 10% nonaethylene glycol monododecyl ether (Sigma Aldrich, St. Louis, MO) dissolved in dichloromethane (wt/vol). Samples were incubated for 5 min at 25°C and taken to dryness at 40°C for 25 minutes to ensure organic solvent was completely evaporated. Pellets contained triglyceride/nonionic surfactant complexes, to which 200 µL of reverse osmosis water was carefully added without mixing and incubated at 40°C for 10 min and followed by a gentle vortex. A standard regression curve was made using 80 nmol of tripalmitin (Sigma Aldrich, St. Louis MO) combined with 25 µL of 10% nonaethylene glycol monododecyl ether in dichloromethane (wt/vol), incubated and dried as above, suspended in 100 µL of reverse osmosis water, and dilutions of 20, 10, 5, 2.5, 1.25, 0.625, and 0.3125 nmol tripalmitin were used. Total TAG from the organic fraction was quantified relative to known tripalmitin standard using a modified colorimetric assay (Van Veldhoven et al., 1997) and are expressed as mM concentrations. Triglyceride Reagent and Free Glycerol Reagent were purchased from Sigma Aldrich (St. Louis, MO) and diluted according to the manufacturer's instructions.

Supplemental Figures

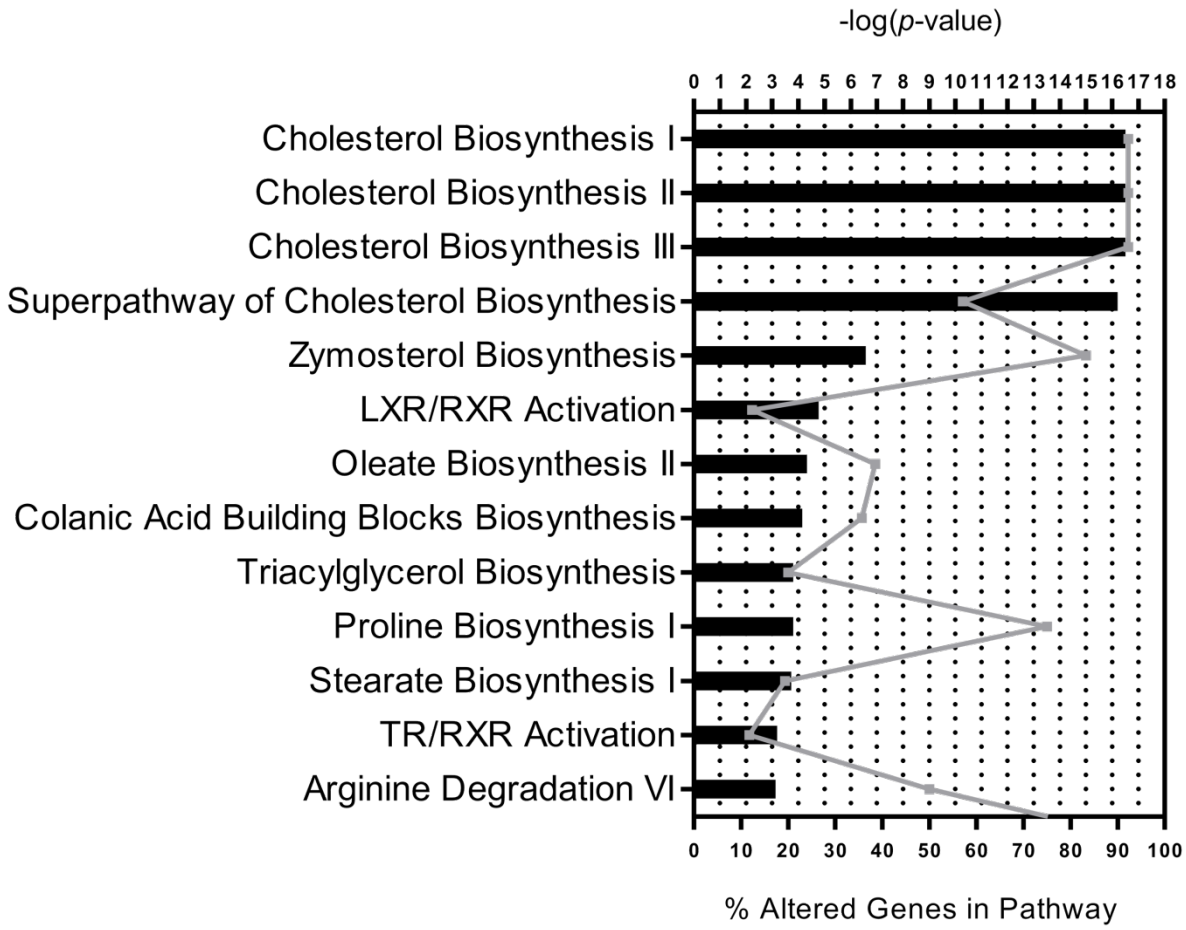

Supplemental Figure 1. Key pathways involved in secretory activation are altered in pregnancy versus lactation. Top 13 pathways represented by mRNAs changed in P14 versus L2 as measured by GeneChip Mouse Gene 1.0 ST array in CD1 mammary epithelial cells analyzed by IPA. Pathways are sorted in order of decreasing statistical significance (-log of *p*-value), represented by black bars with values indicated on the top axis. Grey line represents the percent of genes in each pathway that were altered with values indicated on the bottom axis.

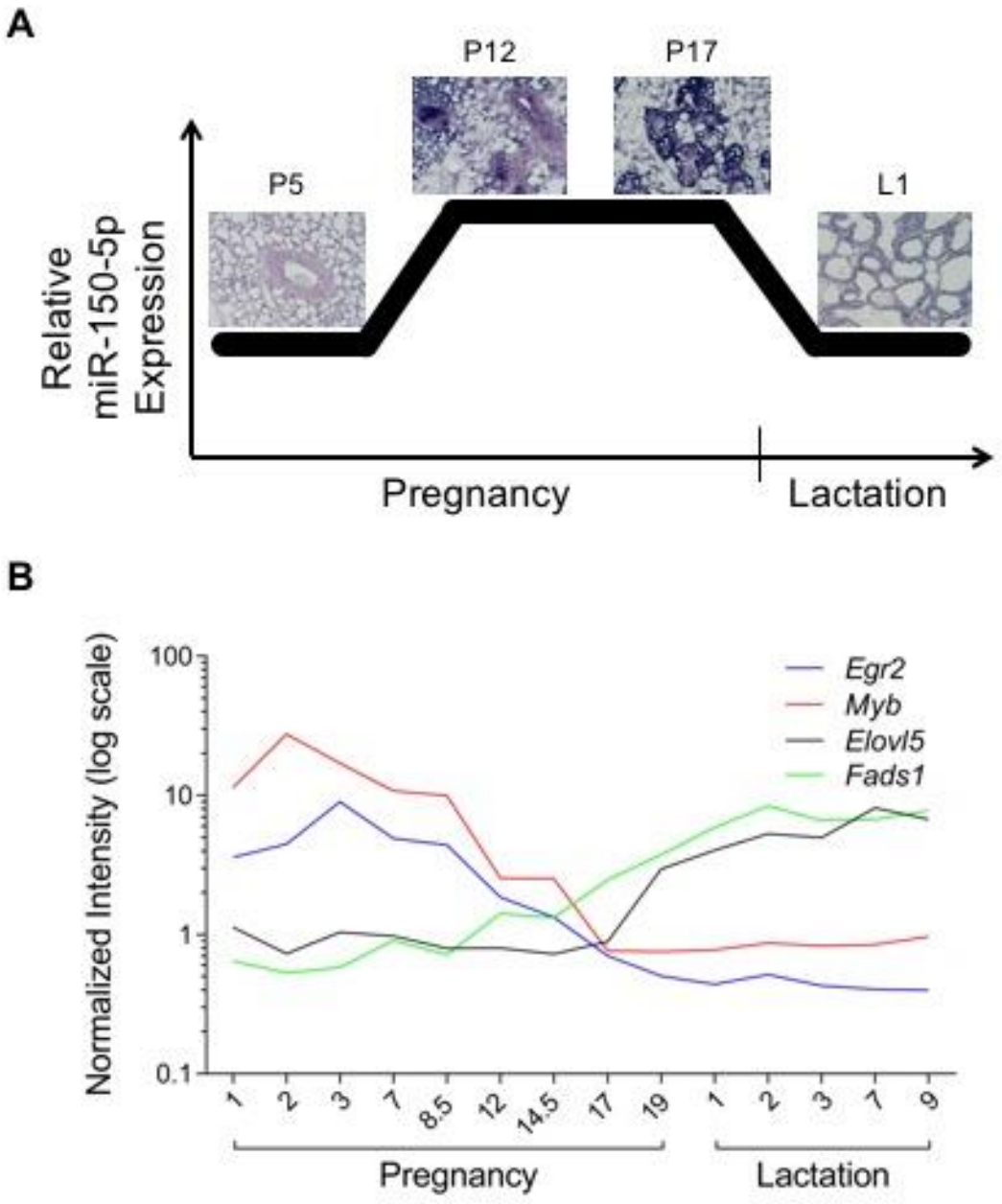

Supplemental Figure 2. miR-150-5p plays a potentially different role at mid-pregnancy. **(A)** A simplified expression pattern of mature miR-150-5p in the normal mammary gland based on ISH performed on whole mammary glands from C57BL/6 mice at P5, P12, P17 and L2, 400× magnification. **(B)** Time course of normalized expression values (log2 transformed) of a selection of validated or predicted miR-150-5p target transcripts from whole mammary gland (4 mice per time point), from a published data set (Rudolph et al., 2003)**.**

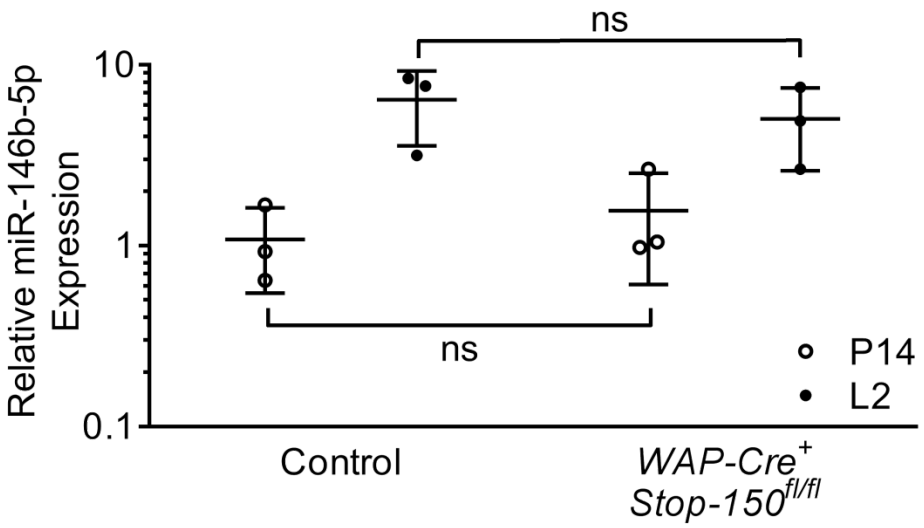

Supplemental Figure 3. Constitutive expression of miR-150 in mammary epithelium throughout lactation did not affect the normal expression pattern of miR-146b-5p, which increases at L2 compared to P14. TaqMan qRT-PCR was used to quantify mature miR-146b-5p expression in RNA isolated from L2 and P14 MECs from the indicated genotype normalized to RNAU6. Error bars represent standard deviation, n=3, unpaired *t*-test.

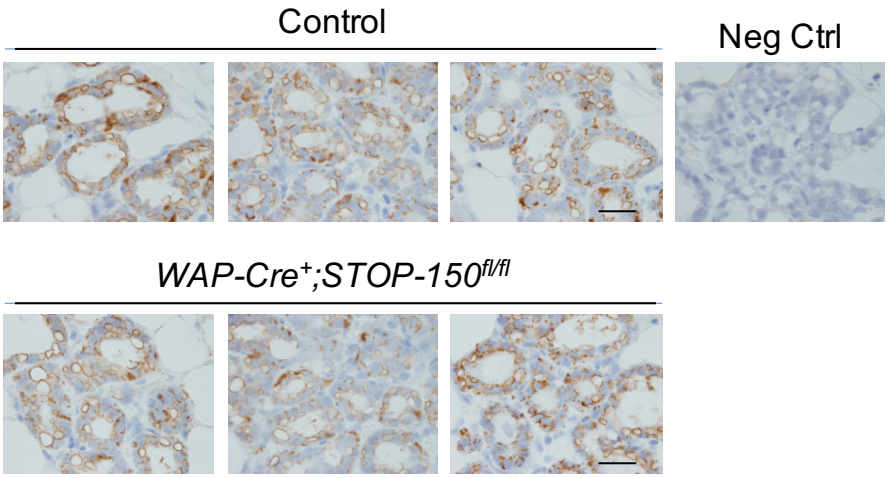

Supplemental Figure 4. Constitutive miR-150 did not suppress lipid droplet formation. IHC for adipophilin in mammary glands at P18 (3 mice per indicated genotype) and negative control (no primary antibody), scale bar = 20μm.

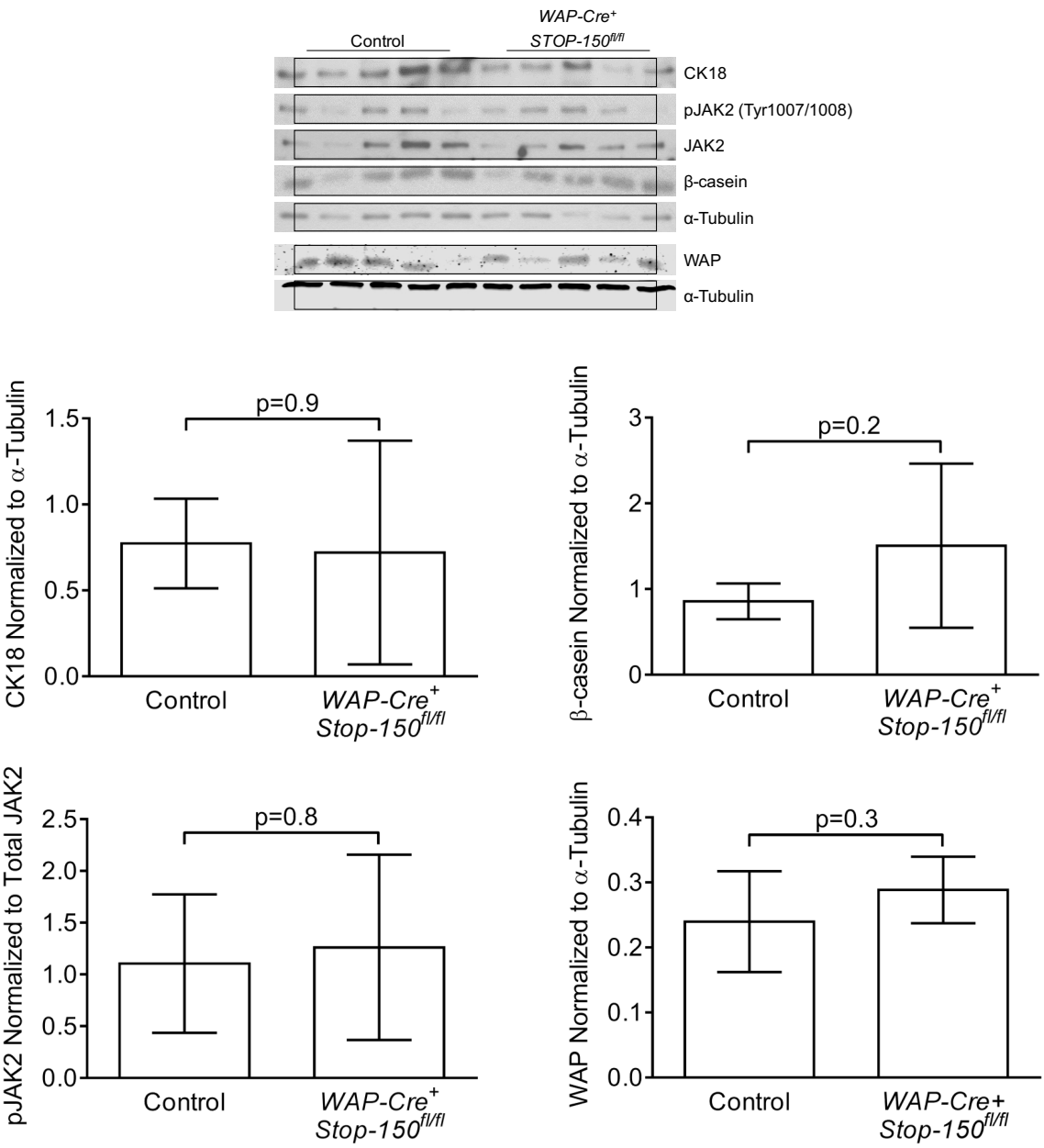

Supplemental Figure 5. Constitutive miR-150 does not affect JAK2 activation or milk protein expression downstream of STAT5. Immunoblot analysis of isolated L2 mammary epithelial cells. Blots were probed with primary antibodies, washed and incubated with appropriate peroxidase-conjugated secondary antibodies, and developed using enhanced chemiluminescence. The primary antibodies used were anti-CK18 (Santa Cruz 28264), anti-pJAK2 (Tyr1007/1008) (Cell Signaling, C80C3), anti-JAK2 (Cell Signaling, D2E12), anti-β-casein (Santa Cruz, 17969), and anti-α-tubulin loading control (Sigma, T5168). Film was scanned using a CanoScan 8600F (Canon, Tokyo, Japan) and densitometry of bands were quantified with ImageJ (National Institutes of Health). Immunoblot for WAP was done by Odyssey infrared imager described in methods.

Supplemental Table 1. Genespring analyzed GeneChip miRNA 1.0 ST data. Affymetrix GeneChip miRNA 1.0 ST microarray results with signal values, *p*-values ($p<0.05$) and fold change for CD1 mammary epithelial cells at pregnancy day 14 versus lactation day 2.

Click here to Download Table S1

Supplemental Table 2. Genespring analyzed GeneChip Mouse Gene 1.0 ST data. Affymetrix GeneChip Mouse Gene 1.0 ST microarray results with signal values, *p*-values ($p<0.05$) and fold change for CD1 mammary epithelial cells at pregnancy day 14 versus lactation day 2.

Click here to Download Table S2

Supplemental Table 3. The majority of significantly downregulated miRNAs at L2 compared to P14 are predicted to target lipid synthesis genes that show a concomitant increase between P14 and L2. Significant downregulated miRNAs are listed on the left, sorted from large to small fold change indicated in parenthesis. Genes involved in lipid synthesis that were TargetScan predicted targets of each miRNA are listed on the right. Numbers in parenthesis indicate fold increase of gene expression at L2 compared to P14 in the Affymetrix Mouse Gene 1.0 ST array. miRNAs that are part of the miR-17/92 cluster are in bold.

Significantly decreased miRNAs predicted to target lipid synthesis genes that increased between P14 and L2

miRNA (-FC)	Predicted Gene Targets (+FC)
miR-150-5p (7.6)	*Olah* (10.7), *Fasn* (6.6), *Fads1* (5.5), *Elovl5* (4.5), *Elovl6* (4.0), *Elovl1* (3.7),
miR-342-3p (4.4)	*Me1* (9.6), *Scd2* (7.2), *Fasn* (6.6), *Fads2* (4.2), *Elovl6* (4.0)
miR-20b-5p (3.8)	*Insig1* (12.1), *Pank3* (3.9)
miR-146a-5p (2.9)	*Fads2* (4.2)
miR-361-5p (2.8)	*Fasn* (6.6), *Scd1* (5.9), *Elovl6* (4.0), *Pank3* (3.9)
miR-342-5p (2.7)	*Scd2* (7.2), *Acly* (4.9)
miR-191-5p (2.6)	*Me1* (9.6), *Elovl6* (4.0)
miR-425-5p (2.5)	*Lpl* (7.8), *Fasn* (6.6), *Elovl5* (4.5), *Thrsp* (4.0), *Pank3* (3.9), *Tpi1* (1.5)
miR-155-5p (2.5)	*Lpl* (7.8), *Fads2* (4.2), *Pank3* (3.9)
miR-18a-5p (2.5)	*Scd2* (7.2), *Acaca* (6.6), *Fads1* (5.5), *Fads2* (4.2), *Elovl1* (3.7)
miR-106a-5p (2.5)	*Insig1* (12.1), *Pank3* (3.9)
miR-17-3p (2.4)	*Acacb* (8.8), *Fasn* (6.6), *Fads1* (5.5), *Acly* (4.9), *Pank3* (3.9)
miR-130b-3p (2.3)	*Slc25a1* (10.9), *Acacb* (8.8), *Elovl6* (4.0)
miR-92a-3p (2.3)	*Insig1* (12.1), *Pank3* (3.9)
miR-17-5p (2.3)	*Insig1* (12.1), *Elovl6* (4.0), *Pank3* (3.9)
miR-150-3p (2.1)	*Insig1* (12.1), *Acaca* (6.6), *Fads1* (5.5), *Elovl6* (4.0), *Pank3* (3.9)
miR-29a-3p (2.1)	*Insig1* (12.1), *Lpl* (7.8), *Scd1* (5.9), *Fads1* (5.5)
miR-20a-5p (2.1)	*Insig1* (12.1), *Pank3* (3.9)
miR-106b-5p (2.1)	*Elovl6* (4.0), *Pank3* (3.9)
miR-15b-5p (2.1)	*Me1* (9.6), *Fasn* (6.6), *Scd1* (5.9), *Fads1* (5.5), *Slc2a1* (3.3)
miR-185-5p (2.1)	*Fads1* (5.5), *Agpat1* (2.1), *Elovl6* (4.0)
miR-106b-3p (2.0)	*Insig1* (12.1), *Elovl6* (4.0), *Pank3* (3.9)
miR-532-5p (2.0)	*Fasn* (6.6), *Acly* (4.9), *Elovl5* (4.5)

Supplemental Table 4. RPPA data. RPPA results include mean net intensities. Individual *p*-values and fold changes comparing control versus WAP-Cre^{+}; Stop-150$^{fl/fl}$ mammary epithelial cells are given for P14 and L2.

Click here to Download Table S4

Supplemental Table 5. Genespring analyzed GeneChip Mouse Transcriptome Assay 1.0 data. Affymetrix GeneChip Mouse Transcriptome Assay 1.0 microarray results with signal values, *p*-values ($p<0.05$) and fold change for CD1 mammary epithelial cells from WAP-Cre^{+}; Stop-150$^{fl/fl}$ mice versus controls at lactation day 2.

Click here to Download Table S5

Supplemental Table 6. The majority of significantly downregulated miRNAs at L2 compared to P14 are predicted to target milk protein genes that show a concomitant increase between P14 and L2. Significant downregulated miRNAs are listed on the left, sorted from large to small fold change indicated in parenthesis. Milk protein genes that were TargetScan predicted targets of each miRNA are listed on the right. Numbers in parenthesis indicate fold increase of gene expression at L2 compared to P14 in the Affymetrix Mouse Gene 1.0 ST array. miRNAs that are part of the miR-17/92 cluster are in bold.

Significantly decreased miRNAs predicted to target milk protein genes that increased between P14 and L2

miRNA (-FC)	**Predicted Gene Targets (+FC)**
miR-150-5p (7.6)	*Egf* (6.7), *Btn1a1* (4.3), *Mfge8* (4.0)
miR-342-3p (4.4)	*Ltf (9.4), Lpo* (8.2), *Xdh* (6.3)
miR-20b-5p (3.8)	*Ltf* (9.4)
miR-146a-5p (2.9)	*Egf* (6.7)
miR-361-5p (2.8)	*Cel* (12.9)
miR-342-5p (2.7)	*Muc1* (8.5), *Egf* (6.7), *Mfge8* (4.0)
miR-140-3p (2.6)	*Egf* (6.7), *Xdh* (6.3)
miR-191-5p (2.6)	*Xdh* (6.3)
miR-425-5p (2.5)	*Ltf* (9.4), *Egf* (6.7), *Btn1a1* (4.3)
miR-155-5p (2.5)	*Egf* (6.7), *Xdh* (6.3), *Btn1a1* (4.3)
miR-18a-5p (2.5)	*Btn1a1* (4.3)
miR-106a-5p (2.5)	*Ltf* (9.4)
miR-17-3p (2.4)	*Ltf* (9.4), *Egf* (6.7)
miR-17-5p (2.3)	*Ltf* (9.4)
miR-150-3p (2.1)	*Btn1a1* (4.3), *Mfge8* (4.0), *Csn1s2b* (1.8)
miR-29a-3p (2.1)	*Wfdc3* (13.1)
miR-185-5p (2.1)	*Xdh* (6.3)
miR-532-5p (2.0)	*Csn2* (1.3)